

Key Points:

- Sea surface cooling is enhanced and storm intensification is suppressed during track-turning stages of tropical cyclones
- The combination of track turning and accompanying slow translation speed results in the cooling enhancement
- Operational forecast models underforecast turning angle and overforecast storm intensity during track-turning stages

Supporting Information:

Supporting Information may be found in the online version of this article.

Correspondence to:

S. Guan,
guanshoude@ouc.edu.cn

Citation:






Guan, S., Liu, P., Zhang, Y., Lin, I.-I., Zhou, L., Yang, Q., et al. (2025). Enhanced sea surface cooling and suppressed storm intensification during slow-moving track-turning stage of tropical cyclones. *Journal of Geophysical Research: Oceans*, 130, e2024JC022234. <https://doi.org/10.1029/2024JC022234>

Received 8 DEC 2024
Accepted 18 JAN 2025

Author Contributions:

Conceptualization: Shoude Guan
Formal analysis: Shoude Guan, Ping Liu, Yihan Zhang, I.-I. Lin, Lei Zhou, Qingxuan Yang, Wei Zhao
Funding acquisition: Wei Zhao
Investigation: Shoude Guan, Ping Liu
Methodology: Ping Liu, Yihan Zhang
Project administration: Wei Zhao
Supervision: Shoude Guan, Qingxuan Yang, Jiwei Tian
Visualization: Ping Liu
Writing – original draft: Shoude Guan, Ping Liu, Yihan Zhang
Writing – review & editing: Shoude Guan, I.-I. Lin, Lei Zhou, Qingxuan Yang

Enhanced Sea Surface Cooling and Suppressed Storm Intensification During Slow-Moving Track-Turning Stage of Tropical Cyclones

Shoude Guan^{1,2,3} , Ping Liu¹, Yihan Zhang¹, I.-I. Lin⁴, Lei Zhou⁵ , Qingxuan Yang^{1,2,3} , Wei Zhao^{1,2,3} , and Jiwei Tian^{1,2,3} 

¹Frontier Science Center for Deep Ocean Multispheres and Earth System (FDOMES) and Physical Oceanography Laboratory/Key Laboratory of Ocean Observation and Information of Hainan Province, Sanya Oceanographic Institution/Academy of Future Ocean, Ocean University of China, Qingdao/Sanya, China, ²Sanya Oceanographic Laboratory, Sanya, China, ³Laboratory for Ocean Dynamics and Climate, Qingdao Marine Science and Technology Center, Qingdao, China, ⁴Department of Atmospheric Sciences, National Taiwan University, Taipei, Taiwan, ⁵School of Oceanography, Shanghai Jiao Tong University, Shanghai, China

Abstract Tropical cyclones (TCs) often undergo track turning when moving over the ocean. However, the influence of track turning on TC-ocean interactions remains little explored. This study systematically investigates sea surface temperature (SST) cooling and TC intensification during TC track-turning stages in global TC-active basins during 1998–2022. Globally, turning TCs induce stronger SST cooling than straight-moving TCs (e.g., -1.53°C vs. -1.08°C for categories 1–2), expand cooling area by 40%–110%, and greatly reduce cooling asymmetry for left-turning (right-turning) TCs in the Northern (Southern) Hemisphere. The translation speed of turning TCs is 1.5 m s^{-1} slower compared to straight-moving TCs. Numerical experiments demonstrate that the enhanced cooling is attributed to the combined effect of track turning and accompanying slow translation speed. The enhanced cooling effectively suppresses storm intensification of turning TCs. The intensification rate for straight-moving versus turning TCs is 2.98 versus 0.06 m s^{-1} per 24 hr for categories 1–2. As turning angle increases, cooling magnitude increases and intensification rate decreases. The probability of rapid intensification for turning TCs is about one-third lower than that for straight-moving TCs. Consequently, TCs with smaller turning angles are more likely to develop into intense TCs. Operational forecast models underforecast turning angles of turning TCs and thus overforecast TC intensity with forecast errors increasing with turning angle. This study demonstrates that TC track-turning stages play a crucial role in modulating TC intensification via an oceanic pathway, highlighting that improving track turning forecast will contribute to enhancing TC intensity forecast accuracy.

Plain Language Summary The movement of tropical cyclones (TCs) is mainly steered by large-scale environmental flow. Under the influence of complex background steering flows in which TCs are embedded, TCs frequently undergo track turning. Theoretically, the track turning can prolong the influencing time of TC's strong wind forcing over local oceans, thus allowing more subsurface cold water to be brought to surface to reduce sea surface temperature. However, systematic analysis is lacking. This study systematically investigates sea surface cooling and TC intensification during TC track-turning stages in global oceans from 1998 to 2022. Turning TCs induce stronger sea surface cooling and are more difficult to intensify compared to straight-moving TCs. Moving speed of turning TCs tends to be slow. Based on numerical experiments, the stronger ocean cooling during track-turning stages is demonstrated to result from the combined effect of track turning and accompanying slow moving speed. Additionally, operational forecasts of turning TCs exhibit large directional deviations from the TC best track and tend to overforecast TC intensity. These findings demonstrate that TC track-turning stages significantly influence sea surface cooling and TC intensification via an oceanic pathway, highlighting the importance of enhancing track turning forecast to improving TC intensity forecast.

1. Introduction

Tropical cyclones (TCs) are among the most destructive natural disasters (Emanuel, 2003, 2005). TCs usually form over the tropical and subtropical oceans and develop by absorbing heat and water vapor from the oceans (Emanuel, 1986). Strong winds of TCs generate near-inertial currents in the upper ocean, whose shear instability triggers intense vertical mixing, entraining colder subsurface water into the mixed layer and resulting in sea

surface temperature (SST) cooling (Guan et al., 2014; Lin et al., 2003; Price, 1983; Shi et al., 2023; Vincent et al., 2012; J. Zhang et al., 2019; X. Zhang et al., 2022). Generally, the vertical entrainment accounts for 75%–90% of the SST cooling, whereas upwelling driven by positive wind stress curl and air-sea enthalpy flux contribute to the remaining SST cooling (Jacob et al., 2000; Potter et al., 2017; Price, 1981; Vincent et al., 2012). The magnitude of SST cooling typically varies from 1°C to 11°C (Chiang et al., 2011; Guan et al., 2021; Lin et al., 2003). In the Northern (Southern) Hemisphere, the SST cooling often exhibits a rightward (leftward) shift relative to the TC track due to the resonance between TC-generated near-inertial currents and clockwise (counterclockwise) rotating TC wind stress (Mei & Pasquero, 2013; Price et al., 1994). TC-induced SST cooling can reduce air-sea enthalpy flux from the ocean to TCs, thereby suppressing the subsequent TC intensification, which is the well-known negative feedback (Balaguru et al., 2012; Cione & Uhlhorn, 2003; Guan et al., 2024; Lin et al., 2013, 2021; Lloyd & Vecchi, 2011; Mei et al., 2012).

The variability of TC attributes, such as intensity, translation speed, and storm size, largely modulates TC-induced SST cooling and the strength of negative feedback (Lin et al., 2009; Liu et al., 2023; Lloyd & Vecchi, 2011; Mei et al., 2012; Mei & Pasquero, 2013; Potter et al., 2017; Pun et al., 2018; Vincent et al., 2012). Lloyd and Vecchi (2011) demonstrated that more intense TCs produce stronger ocean cooling up to category 2 but produce less or approximately equal cooling for categories 3–5. Mei et al. (2012) showed that slower-moving TCs induce stronger SST cooling and have longer exposure to the cooling, both of which strengthen the suppressing effect of cooling on TC intensification. Liu et al. (2023) reported that larger TCs tend to induce stronger SST cooling and thus their intensification is suppressed to a greater extent. Additionally, TC-induced SST cooling is stronger for ocean stratification with shallower mixed layer, leading to stronger suppression of TC intensification (Lin et al., 2009; Vincent et al., 2012; G. Wang et al., 2016). Multiscale ocean processes, including mesoscale eddies (Jaimes & Shay, 2010; Shay et al., 2000), the barrier layer (Balaguru et al., 2012; Jyothi et al., 2022), and internal tides (Guan et al., 2024), can also modulate the cooling effect and thus influence TC intensification.

TC movement is primarily steered by large-scale environmental flows (Chan, 2005; Chan & Gray, 1982; K. Gao et al., 2023; George & Gray, 1977), which are modulated by various processes, such as the subtropical high and the monsoon trough (Bi et al., 2020; Lin & Chan, 2015). Under complex and variable steering flows, TC movement has large variability often manifested by frequent track turning (Camargo et al., 2007; Chan et al., 1980). Previous studies mainly focused on atmospheric environment fields and mechanisms behind track turning (e.g., Camargo et al., 2007; Chan et al., 1980; Wu et al., 2013). Recent case studies reported that ocean cooling during TC track-turning stages tends to be enhanced (e.g., D'Asaro et al., 2014; Li et al., 2021; Pun et al., 2018; H. Zhang et al., 2023; Y. Zhang et al., 2023). D'Asaro et al. (2014) proposed that Typhoon Lupit (2009) induced strong SST cooling near its northward turning. By employing numerical experiments, Pun et al. (2018) demonstrated that the track turning of Typhoon Megi (2010) contributed 30% to total SST cooling. Li et al. (2021) revealed that during sharp left-turning stage of Typhoon Nida (2009), SST cooling was ~5°C stronger than during straight-moving stage with similar typhoon intensity. H. Zhang et al. (2023) reported that Typhoon Nakri (2019) induced stronger SST cooling in a warm-eddy region than in a cold-eddy region because of Nakri's track turning over the warm eddy. H. Wang et al. (2023) found that super typhoon Hinnamnor (2022) induced SST cooling of ~5.6°C during its sudden track-turning stage, leading to rapid weakening of the typhoon's intensity with maximum wind speed decreasing by 22 knots in 6 hr.

Although previous case studies suggest enhanced ocean cooling during track-turning stages of TCs, the global statistical characteristics of the magnitude and spatial structure of SST cooling as well as the underlying mechanism remain unclear. Additionally, the influence of modulated cooling on TC intensification and rapid intensification is rarely known. This study aims to systematically characterize the SST response and storm intensification during track-turning stages based on global TCs in the past 25 years. Our results reveal stronger SST cooling, larger cooling area, and modulated left-right asymmetry of cooling for turning TCs compared to straight-moving ones. Using numerical experiments, the cooling enhancement is demonstrated to result from the combination of track turning and accompanying slow translation speed. Furthermore, the enhanced cooling effectively suppresses TC intensification and lowers the probability of rapid intensification during track-turning stages. Additionally, operational forecast models tend to underforecast track turning and overforecast TC intensity during track-turning stages.

The structure of the paper is organized as follows: Section 2 introduces the data and methods. Section 3 compares SST cooling between turning and straight-moving TCs, explores the underlying mechanism for modulated

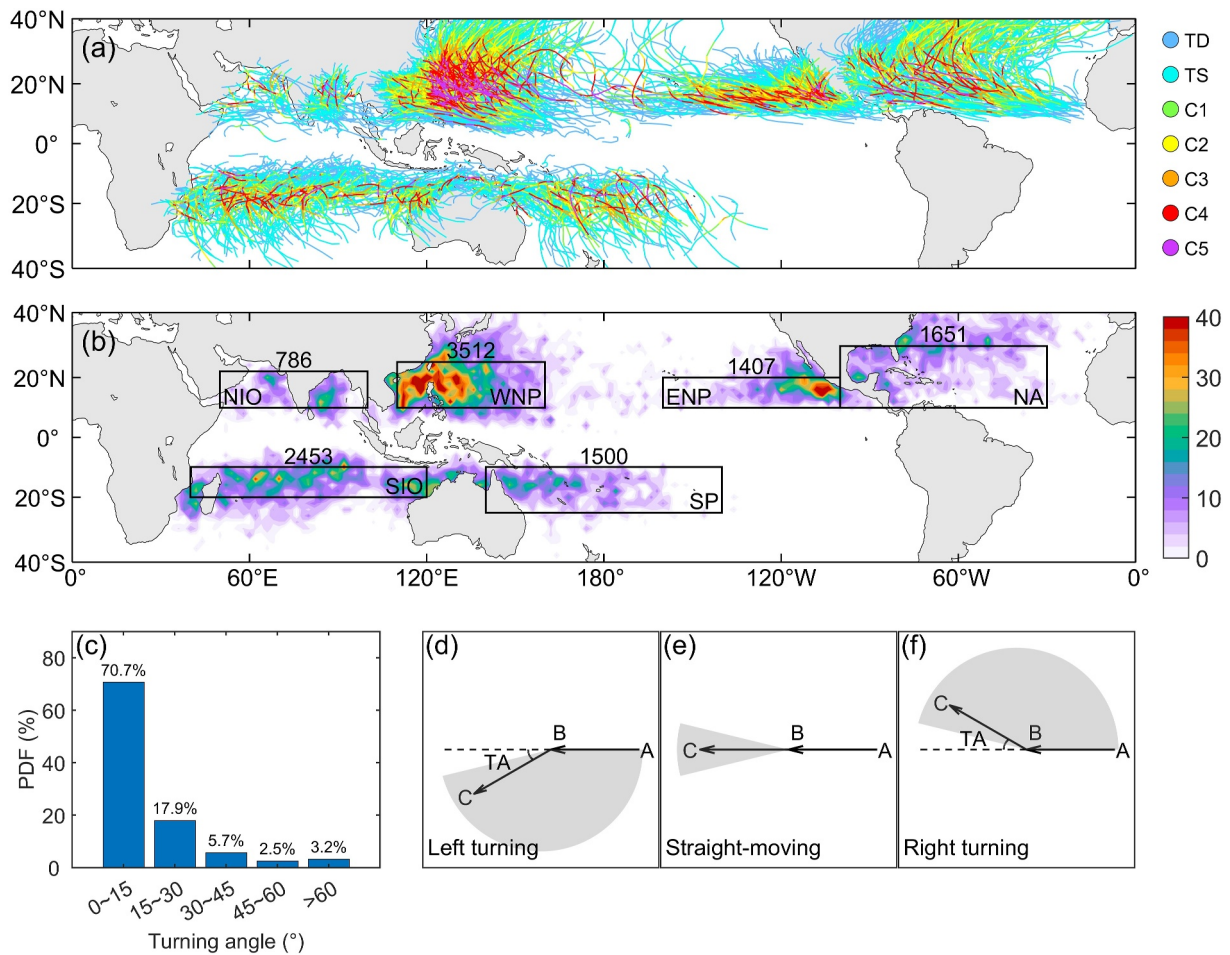


Figure 1. (a) Tropical cyclone (TC) tracks during 1998–2022. Different colors indicate different categories of TC intensity: tropical depression (TD), tropical storm (TS), and categories 1–5 (C1–C5). (b) The number of turning track points (turning angle > 15°) within 2° × 2° boxes. Black boxes denote TC-active basins. The number of turning track points in each TC-active basin is shown above the corresponding black box. (c) The probability distribution function (PDF) of TC turning angle in global oceans. (d)–(f) Diagram of definitions of left-turning, straight-moving, and right-turning TC track points. The gray shading areas indicate their respective turning angle range. A, B, and C denote TC track points at –6 hr, 0 hr, and 6 hr relative to the current track point, respectively. TA is the abbreviation for turning angle.

cooling by turning TCs based on numerical experiments, and examines the negative feedback to TC intensification. Section 4 discusses forecast errors of turning TCs. Finally, the main findings are summarized in Section 5.

2. Data and Methods

2.1. TC Best Track Data

TC best track data are obtained from the International Best Track Archive for Climate Stewardship (IBTrACS; Knapp et al., 2010), distributed by the Joint Typhoon Warning Center (JTWC) and the National Hurricane Center (NHC), providing TC center position and maximum wind speed (V_{\max} , m s^{-1}) at 6-hr intervals. A total of 2,123 TCs in global oceans from 1998 to 2022, with more than 47,000 track points over the ocean, are involved in composite analyses (Figure 1a). TC intensity is classified into seven categories on the Saffir-Simpson scale (Webster et al., 2005): tropical depression (TD), tropical storm (TS), and categories 1–5 (C1–C5). The intensification rate (IR), a metric that measures TC intensity change, is defined as the V_{\max} change in the subsequent 24 hr after passing the current position (unit: m s^{-1} per 24 hr). The translation speed (U_h) is calculated by dividing the moving distance between 6 hr before and 6 hr after the current position by the time interval (12 hr). To rule out the landmass effect, TC track points within 24 hr before landfall have been pre-excluded.

The direction of TC movement relative to due east is defined as the direction angle (DA) with a positive value indicating a counterclockwise angle from due east to the TC moving direction. To quantify the directional change of TC movement, we define the turning angle as the difference in DA between the current track point and the one 6 hr earlier, that is, $\text{turning angle}(t_0) = \text{DA}(t_0) - \text{DA}(t_0 - 6 \text{ hr})$ as illustrated in Figures 1d–1f. A positive turning angle signifies left turning, whereas a negative turning angle signifies right turning. Results show that approximately 30% of turning angles in global oceans exceed 15° in magnitude (Figure 1c), varying from 18% to 39% across TC-active basins (Figure S1 in Supporting Information S1). In this study, left-turning and right-turning TCs are identified when turning angle is smaller than -15° and larger than 15° , respectively (Figures 1d and 1f). A straight-moving TC is identified when the turning angle falls between -15° and 15° (Figure 1e). Unless specifically noted as left or right turning, turning TCs refer to the combination of left- and right-turning TCs. Hereafter, value of turning angle refers to its absolute value except for negative turning angle forecast errors in Section 4.

We examine TC-induced SST cooling and TC intensification in global TC-active basins (Figure 1b), including six individual basins as defined below: the western North Pacific (WNP): $10^\circ\text{--}25^\circ\text{N}$, $110^\circ\text{--}160^\circ\text{E}$; the eastern North Pacific (ENP): $10^\circ\text{--}20^\circ\text{N}$, $100^\circ\text{--}160^\circ\text{W}$; the North Atlantic (NA): $10^\circ\text{--}30^\circ\text{N}$, $30^\circ\text{--}100^\circ\text{W}$; the north Indian Ocean (NIO): $10^\circ\text{--}22^\circ\text{N}$, $50^\circ\text{--}100^\circ\text{E}$; the South Pacific (SP): $10^\circ\text{--}25^\circ\text{S}$, $140^\circ\text{E--}140^\circ\text{W}$; the south Indian Ocean (SIO): $10^\circ\text{--}20^\circ\text{S}$, $40^\circ\text{--}120^\circ\text{E}$. Additionally, we also composite SST cooling and TC intensification on global and two hemispheric averages (the Northern Hemisphere, NH; the Southern Hemisphere, SH).

Generally, TC track turning occurs widely across all TC-active basins with notable concentrations in the WNP and ENP (Figure 1b), which is possibly related to the prevailing subtropical high (Bi et al., 2020). The WNP records the highest number of turning track points (3,512) followed by the SIO (2,453). In contrast, the NIO (786) has the fewest turning track points (786) due to its low TC frequency. The number of turning track points is comparable in the NA (1,651), ENP (1,407), and SP (1,500). Regarding the probability of track turning, the NIO and SP exhibit the highest likelihoods (39% and 37%), whereas the ENP has the lowest probability (18%), followed by the NA (24%; Figure S1 in Supporting Information S1). Hemispheric averages indicate a higher probability of track turning in the SH compared to the NH (38% vs. 26%).

2.2. SST Observations

To investigate SST responses to TCs, the optimally interpolated (OI) SST product (daily, spatial resolution of $0.25^\circ \times 0.25^\circ$) is obtained from the Remote Sensing Systems (RSS). This SST product is derived from microwave radiometer measurements, which can penetrate clouds and provide reliable SST data even under TC conditions (Wentz et al., 2000). The SST data are available since 1998, and for consistency, all data used in the composite analyses span the period from 1998 to 2022. The long-term linear trend and climatological seasonal cycle are extracted from the original SST data at each grid cell and subsequently removed by subtracting these components from the original data. Pre-TC SST is defined as the average SST of 12 to 3 days before TC passage. The SST anomaly (SSTA) is calculated by the post-TC SST (average SST during 1–3 days after TC passage) minus the pre-TC SST. The spatial pattern of SSTA in TC-centric coordinate system is composited following Mei and Pasquero (2013) and Liu et al. (2023). For each 6-hr TC track point, we define a domain centered on the TC center with edges oriented parallel or perpendicular to the TC moving direction. The size of the domain is $1,000 \text{ km} \times 1,000 \text{ km}$, and the grid within the domain is constructed with a spatial resolution of $10 \text{ km} \times 10 \text{ km}$. The SST data are then linearly interpolated onto these grids.

2.3. Reanalysis Data

To calculate the vertical wind shear (VWS), wind data are obtained from the ERA5 database distributed by the European Centre for Medium-Range Forecasts (ECMWF) (Hersbach et al., 2023). The VWS is defined as the difference in the mean wind vectors within 200–800 km from the TC center between 200 and 850 hPa levels (Chen et al., 2006; DeMaria, 1996).

2.4. TC Forecast Data

Considering that SST cooling and negative feedback to TC intensification are modulated during track-turning stages, forecasts of TC intensity may also be affected. Therefore, we compare forecast errors between turning and straight-moving TCs using operational forecast data issued by the NHC. The forecast data include forecast

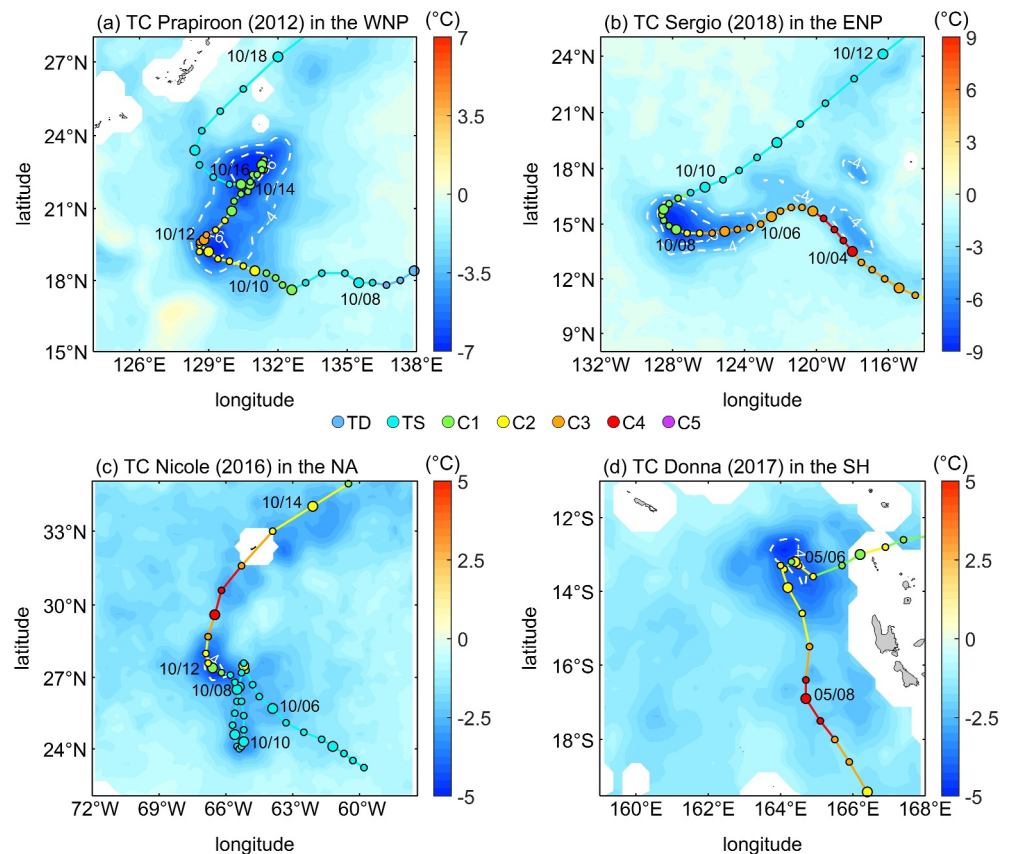


Figure 2. Maximum SST cooling induced by (a) TC Prapiroon (2012) in the WNP during 6–19 October 2012, (b) TC Sergio (2018) in the ENP during 2–12 September 2018, (c) TC Nicole (2016) in the NA during 4–15 October 2016, and (d) TC Donna (2017) in the SH during 2–11 May 2017. The respective pre-TC SST is calculated by averaging SST from 3 to 5 days prior to 6 October 2012, 2 September 2018, 4 October 2016, and 2 May 2017. Colored lines and dots denote TC tracks, with larger dots representing TC track points at 0000UTC each day.

position and 1-min V_{\max} for TCs in the ENP and NA since 1998. The forecast data, issued every 6 hr, contain projections valid 12, 24, 36, 48, 72, 96, and 120 hr after the forecast's initial time (0000, 0600, 1,200, and 1,800 UTC, respectively). In Section 4, we estimate forecast errors of turning angle and V_{\max} , calculated by the forecast value minus the best track value. We also calculate TC track forecast errors, defined as the distance between the forecast position and the best track position. Considering that the forecast interval is at least 12 hr, the turning angle in Section 4 is defined as the difference in DA between the current track point and the one 12 hr earlier, that is, turning angle (t_0) = DA(t_0) – DA(t_0 –12 hr).

3. Results

3.1. Enhanced Sea Surface Cooling During Track-Turning Stages of TCs

3.1.1. Case Study

To explore the potential effect of TC track turning on sea surface cooling, we first examine SST cooling associated with four TC cases characterized by obvious track turning (Figure 2). The four TCs are TC Prapiroon (2012) in the WNP, TC Sergio (2018) in the ENP, TC Nicole (2016) in the NA, and TC Donna (2017) in the SH. All four TCs induce notable SST cooling along their tracks with larger cooling occurring predominantly to the right of TC tracks in the NH and to the left in the SH. Quantitatively, SST cooling along the straight tracks, where TC intensity reached up to category 4, is weaker than -3.66°C for Prapiroon, -4.14°C for Sergio, -2.80°C for Nicole, and -2.34°C for Donna. By comparison, prominent SST cooling patches are observed along the turning tracks of these TCs, with respective cooling of approximately -6.88°C , -8.69°C , -4.72°C , and -4.39°C , despite that TC intensity is limited to category 3. In particular, Prapiroon exhibits weaker intensity during the second

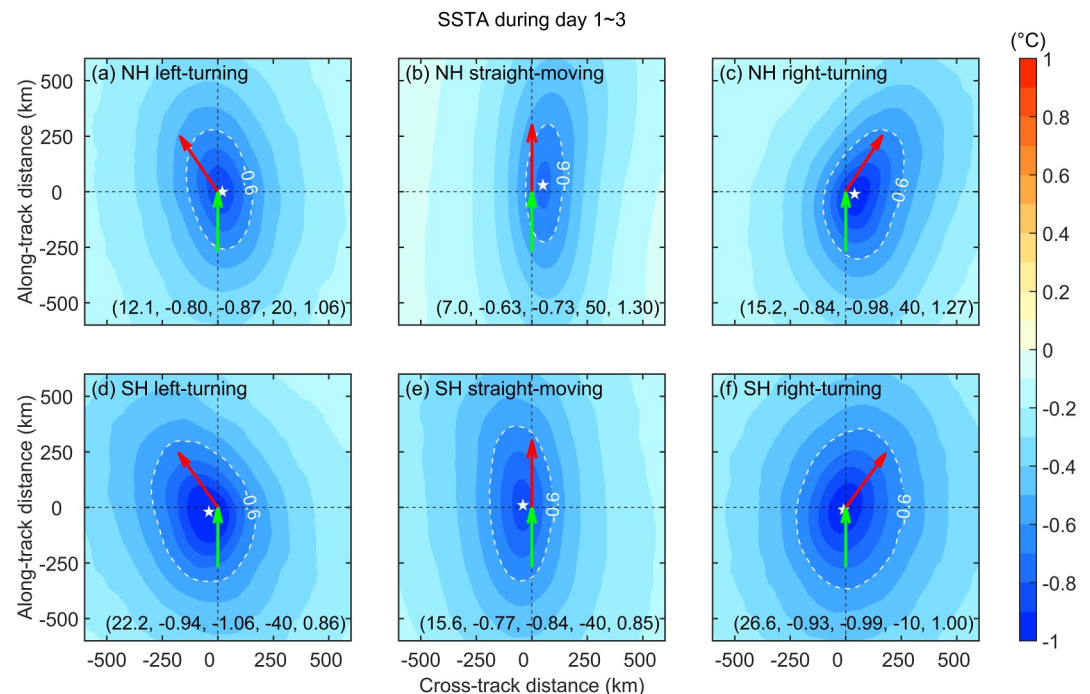


Figure 3. Spatial pattern of TC-induced SSTA in TC-centric coordinate associated with (a) and (d) left-turning, (b) and (e) straight-moving, and (c) and (f) right-turning TCs in the (a, b, and c) Northern Hemisphere (NH) and (d, e, and f) Southern Hemisphere (SH). The center of the coordinate indicates the TC center position. The green arrow indicates the moving direction in the past 6 hr. The red arrow indicates the average moving direction in the next 6 hr. The pentagram represents the location of maximum SST cooling. The values in parentheses at the bottom indicate the area of SSTA stronger than -0.6°C ($\times 10^4 \text{ km}^2$), the average SSTA within 100 km from the TC center ($^{\circ}\text{C}$), the minimum SSTA ($^{\circ}\text{C}$), the x -axis location of the minimum SSTA (km), and the asymmetric index, respectively.

turning stage (14–16 October 2012) compared to the first turning stage (11–12 October 2012). However, SST cooling during the second turning stage is stronger and covers a larger area (Figure 2a) likely due to the larger turning angle ($\sim 180^{\circ}$) during this stage. The 180° track turning allows TC wind forcing to revisit previously cooled regions, thereby enhancing cooling. Additionally, the TC translation speed (i.e., U_h) during track-turning stages is relatively slow for each TC case. Therefore, the prominent SST cooling during track-turning stages mainly results from the combined effect of track turning and slow U_h , which prolongs the duration of TC wind forcing, facilitating mixing and upwelling (Densmore et al., 2023; Lin et al., 2009; Mei et al., 2012; H. Zhang et al., 2023).

Theoretically, enhanced SST cooling can reduce air-sea enthalpy flux from the ocean to TCs, thereby suppressing subsequent TC intensification (D'Asaro et al., 2014; Emanuel, 2003; Lin et al., 2013). Additionally, track turning and slow U_h can prolong exposure of TCs to cooling regions, which further contributes to the suppression of TC intensification (Bender & Ginis, 2000; Lin et al., 2009; Liu et al., 2023). Observations show that Prapiroon and Sergio exhibit an obvious decrease in intensity following their track-turning stages. Specifically, for Prapiroon, V_{\max} decreases by 12.9 and 10.3 m s^{-1} within 24 hr after the first and second turning stages, respectively. For Sergio, V_{\max} decreases by 7.7 m s^{-1} within 24 hr after passing the cooling region associated with track turning. However, Nicole and Donna do not exhibit a decrease in intensity probably due to favorable atmospheric conditions.

3.1.2. Compositing SST Cooling

The above TC cases preliminarily demonstrate cooling enhancement and suppression of storm intensification during track-turning stages. To assess the robustness of these phenomena, we perform composite analyses based on global TCs during 1998–2022. Figure 3 presents the spatial patterns of SSTA induced by left-turning, straight-moving, and right-turning TCs. The average turning angle of both left- and right-turning TCs is approximately 35° .

as indicated by red arrows in Figure 3. In the NH, the maximum SST cooling is -0.73°C for straight-moving TCs but is enhanced to -0.87°C for left-turning TCs and -0.98°C for right-turning TCs (Figures 3a–3c). In the SH, the maximum SST cooling for straight-moving TCs is -0.84°C , which is enhanced to -1.06°C for left-turning TCs and -0.99°C for right-turning TCs (Figures 3d–3f). We also calculate the average SSTA within 100 km (approximately twice the global average radius of V_{max}), which largely determines air-sea enthalpy flux from the ocean to TCs and negative feedback onto TC intensification. For straight-moving TCs, the average SSTA is -0.63°C in the NH and -0.77°C in the SH. By comparison, both left- and right-turning TCs induce stronger SSTA within 100 km (-0.80°C and -0.84°C in the NH; -0.94°C and -0.93°C in the SH). These results suggest that in the NH, right-turning TCs result in stronger SST cooling enhancement compared to left-turning TCs, whereas in the SH, left-turning TCs result in stronger cooling enhancement than right-turning TCs. Additionally, the area of SST cooling is extended during track-turning stages. For left- and right-turning TCs, the respective area with SSTA stronger than -0.6°C is approximately 1.7 and 2.1 times that for straight-moving TCs in the NH (Figures 3a–3c) and 1.4 and 1.7 times in the SH (Figures 3d–3f).

We also examine the influence of track turning on the left-right asymmetry of SSTA. In the NH, the maximum SST cooling induced by straight-moving TCs manifests a 50-km rightward shift relative to the TC track (Figure 3b), which is consistent with previous studies (e.g., Mei & Pasquero, 2013; Price et al., 1994). Similarly, maximum cooling shifts 40 km rightward for right-turning TCs (Figure 3c). However, maximum cooling only shifts 20 km to the right of the TC track for left-turning TCs (Figure 3a). In the SH, the maximum SST cooling induced by straight-moving TCs manifests a 40-km leftward shift relative to the TC track, which decreases to 10 km for right-turning TCs but remains unchanged for left-turning TCs (Figures 3d–3f). Cooling contours exhibit different patterns for straight-moving and turning TCs. For straight-moving TCs, cooling contours in front of the TC are generally parallel to the TC track (Figures 3b and 3e). However, for left-turning (right-turning) TCs, cooling contours in front of the TC manifest a left (right) bias, following the bias of TC wind fields, in both the NH and SH (Figure 4). To further quantify the left-right asymmetry of SSTA during track-turning stages, we define an asymmetric index as follows:

$$\text{asymmetric index} = \frac{\int_0^{100} \text{SSTA} \, dx}{\int_{-100}^0 \text{SSTA} \, dx} \quad (y = 0) \quad (1)$$

where x and y are coordinates perpendicular and parallel to the TC track in the TC-centric coordinate system. For straight-moving TCs in the NH (SH), strong cooling is predominately located to the right (left) side of the TC track, yielding an asymmetric index of 1.30 (0.85) (Figures 3b and 3e). Strong cooling associated with left-turning TCs in the NH is shifted leftward but is still predominately located to the right, resulting in a decrease of the asymmetric index to 1.06 (Figure 3a). In contrast, strong cooling associated with right-turning TCs in the SH is shifted rightward, with the asymmetric index increasing to 1.00, indicating a nearly symmetric cooling pattern (Figure 3d). However, the influence of right (left) turning in the NH (SH) on SSTA asymmetry is minimal (Figures 3c and 3f). The results align with the position of maximum SST cooling during TC track-turning stages. Similar results are also observed in each TC-active basin, where the left-right asymmetry of SSTA is greatly reduced during left-turning (right-turning) stages for basins in the NH (SH) (Figure S2 in Supporting Information S1). The spatial pattern of SSTA influences the overlying deep convection and TC structure, subsequently affecting the spatial distribution of rainfall (Ma et al., 2023; Ye et al., 2023). Thus, the modulated spatial pattern of cooling during track-turning stages may potentially alter TC structure and rainfall distribution.

Considering that TC-induced SSTA strongly depends on TC intensity (Lloyd & Vecchi, 2011; Mei & Pasquero, 2013), we categorize TCs into three groups: tropical depression and tropical storms (TD–TS), categories 1–2, and categories 3–5. The SSTA averaged within 100 km from the TC center is composited in different TC-active basins (Figure 4). On a global average, turning TCs induce stronger SST cooling than straight-moving TCs in each group (e.g., -1.53°C vs. -1.08°C for categories 1–2), all significantly above the 99% confidence level. Compared to straight-moving TCs, the global average SSTA amplitude induced by turning TCs is increased by 0.21°C (46.1%), 0.45°C (41.9%), and 0.37°C (27.4%) for TD–TS, categories 1–2, and categories 3–5 TCs, respectively. The largest increase in SSTA amplitude occurs for categories 1–2 TCs and the smallest for TD–TS.

Similar results are found across each TC-active basin and hemispheric averages. Among global TC-active basins, the largest increase in SSTA amplitude during track-turning stages occurs in the ENP (0.68°C for categories 1–2).

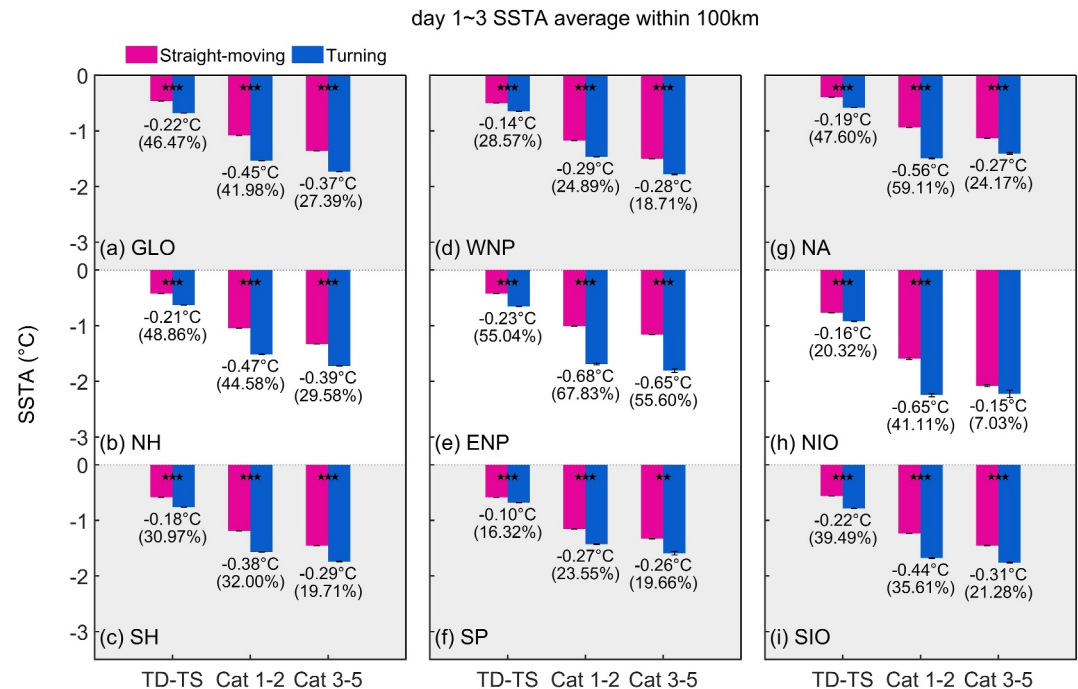


Figure 4. Comparison of TC-induced SSTA between straight-moving and turning TCs in TC-active basins. Average SSTA within 100 km from the TC center associated with straight-moving (red) and turning (blue) TCs in panel (a) global oceans (GLO), (b) the Northern Hemisphere (NH), (c) the Southern Hemisphere (SH), (d) the western North Pacific (WNP), (e) the eastern North Pacific (ENP), (f) the South Pacific (SP), (g) the North Atlantic, (h) the north Indian Ocean (NIO), and (i) the south Indian Ocean (SIO). Error bars indicate the 95% confidence interval. Pentagrams indicate the confidence level of SSTA difference between turning and straight-moving TCs: one pentagram suggests the difference is significant above the 90% confidence level, two for 95%, and three for 99% based on the Student's *t* test. The SSTA difference and its percentage with respect to SSTA induced by straight-moving TCs are shown behind bars.

For categories 1–2 TCs in the NIO and NA, the increases in SSTA amplitude are also significantly considerable (0.65°C and 0.56°C). Nevertheless, the SSTA induced by categories 3–5 TCs in the NIO shows no significant difference between turning and straight-moving TCs likely due to the insufficient sampling size of TCs for statistical significance test. Generally, the enhancement of SST cooling during track-turning stages is more pronounced in the NH than in the SH (e.g., 0.47°C vs. 0.38°C for categories 1–2 TCs).

3.1.3. Mechanism

Previous case studies indicated that TC *U_h* during track-turning stages tends to be slow (e.g., Densmore et al., 2023; Li et al., 2021; Pun et al., 2018; H. Zhang et al., 2023). Densmore et al. (2023) emphasized the importance of both track turning and slow *U_h* to the mechanism behind upper-ocean response to TCs. Both track turning and slow *U_h* can prolong the local residence time of TC wind forcing, facilitating mixing driven by kinetic energy input and upwelling driven by Ekman suction, which contributes to sea surface cooling (Densmore et al., 2023; Mei et al., 2012; H. Zhang et al., 2023). Furthermore, some case studies quantified the relative contribution of track turning to SST cooling through numerical experiments with results varying among different TC cases. For instance, the track turning of Typhoon Megi (2010) and Typhoon Prapiroon (2012) accounts for 30% and 40% of the total SST cooling, respectively (Pun et al., 2018; Y. Zhang et al., 2023). However, these studies focus on individual TC cases and do not yield robust conclusions that can be generalized across all TC scenarios. Therefore, we statistically investigate the underlying mechanisms behind the enhancement of SST cooling during TC track-turning stages based on TCs during 1988–2022.

The occurrence of TC track turning is closely related to *U_h* over global oceans (Figure 5). As TCs slow down, the turning angle increases, leading to a higher probability of track turning (Figures 5b and 5c). When *U_h* is lower than 2 m s^{−1}, the global average turning angle is 30°, and the percentage of track turning reaches up to 62%. In contrast, when *U_h* exceeds 6 m s^{−1}, the average turning angle is smaller than 8°, and the percentage of track

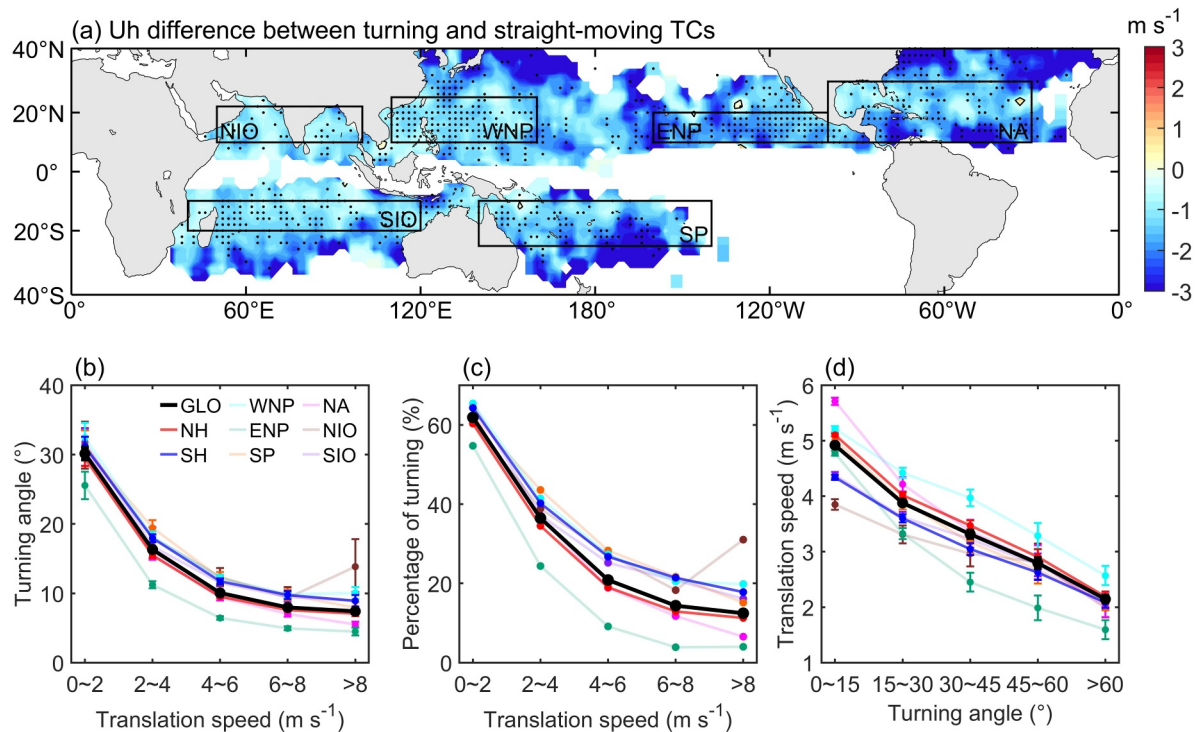


Figure 5. (a) Difference in translation speed between turning and straight-moving TCs within $2^\circ \times 2^\circ$ boxes. Black dots indicate the difference is above the 90% confidence level. Black boxes denote TC-active basins. (b) TC turning angle as a function of translation speed in global and TC-active basins. Error bars represent the 95% confidence interval. (c) Percentage of track turning as a function of translation speed in global and TC-active basins. (d) TC translation speed as a function of turning angle in global and TC-active basins. Error bars represent the 95% confidence interval.

turning drops below 14%. Similarly, U_h decreases as the turning angle increases (Figure 5d). The global average U_h is 4.9 m s^{-1} for turning angles smaller than 15° but decreases to 2.1 m s^{-1} when turning angle exceeds 60° . Overall, TC track turning is typically accompanied by slow U_h . The relationship between turning angle and U_h in individual TC-active basins is consistent with the global average. Physically, the slow U_h accompanying TC track turning is likely attributed to weak environmental steering flows around TCs, which are related to the weakening subtropical high and deepening westerly trough (e.g., Camargo et al., 2007; Wu et al., 2013). Consequently, turning TCs exhibit lower U_h than straight-moving TCs in most regions (3.5 m s^{-1} vs. 5.0 m s^{-1}) with an average U_h difference of 1.5 m s^{-1} (Figure 5a). The combination of track turning and slow U_h can prolong the local residence time of TC wind forcing, contributing to cooling enhancement during slow-moving track-turning stages (Densmore et al., 2023; Li et al., 2021; Pun et al., 2018; H. Zhang et al., 2023).

To further investigate and quantify the contribution of track turning and slow U_h to cooling enhancement, we conduct a series of numerical experiments by employing the three-dimensional Price-Weller-Pinkel model (3DPWP; Price et al., 1994), which has been widely used in TC-ocean interaction studies (e.g., Balaguru et al., 2015; Guan et al., 2014; Lin et al., 2013; Pun et al., 2018; Walker et al., 2014; Ye et al., 2023; H. Zhang et al., 2023). The model is configured with horizontal grids at a resolution of $5 \text{ km} \times 5 \text{ km}$, covering a domain size of $2,000 \text{ km} \times 2,000 \text{ km}$. In the vertical direction, the domain extends to a depth of 1,000 m and is divided into 45 layers, with a 5-m interval of the first 20 layers, a 10-m interval of the middle 10 layers, and a 50-m interval of the last 15 layers. The time step is 600 s. The f -plane is utilized with the latitude set at 20°N . A series of experiments are designed (Table 1). In the first two experiments, the TCs move along a straight path at constant U_h of 5.0 m s^{-1} and 3.5 m s^{-1} (Figures S3a and S3b in Supporting Information S1), which are average U_h of turning and straight-moving TCs, respectively. Subsequent experiments are divided into two groups with TCs undergoing left and right turning, respectively. The turning angle ranges from 30° to 180° in increments of 30° (Figures S3c–S3n in Supporting Information S1). In both groups, the TC U_h remains constant at 3.5 m s^{-1} . Throughout all experiments, the maximum wind speed of TCs is set as 35 m s^{-1} (category 1 TC), and the radius of maximum wind

Table 1
Settings of Tropical Cyclones in Numerical Experiments

Track direction	Straight moving				Right turning					Left turning				
Translation speed (m s^{-1})	5.0	3.5	3.5	3.5	3.5	3.5	3.5	3.5	3.5	3.5	3.5	3.5	3.5	3.5
Turning angle	0°	0°	30°	60°	90°	120°	150°	180°	30°	60°	90°	120°	150°	180°

speed is 60 km. The initial temperature and salinity profile are extracted from climatological monthly World Ocean Atlas data (Figure S4 in Supporting Information S1).

Figure 6 shows the spatial pattern of simulated SSTA induced by TCs. The SSTA is calculated by subtracting the initial SST from the average SST during days 1–3 after TC passage. For the straight-moving TC with fast Uh (5.0 m s^{-1}), the maximum cooling is located 50 km to the right of the TC track (Figure 6a), consistent with observations in the NH (Figure 3a). As TC slows down ($Uh = 3.5 \text{ m s}^{-1}$), the rightward shift of the maximum cooling decreases to 40 km (Figure 6b). The reduced shift occurs because the ocean response becomes increasingly dominated by upwelling as Uh decreases, and upwelling is symmetrical around the TC track (Densmore et al., 2023; Price, 1981). In addition to Uh, track turning also influences the position of maximum cooling. Compared to the cooling induced by the straight-moving TC with slow Uh, right turning shifts the maximum cooling rightward by 10 km for turning angles of 30°–90° but shifts the maximum cooling leftward by 30 km for a 150° turning angle (Figures 6c–6g). For left turning, the maximum cooling position remains unaffected for turning angles of 30°–60° (Figures 6i and 6j). However, for turning angles of 90°–150°, left turning shifts the maximum cooling leftward by 55–70 km, leading to a leftward-biased SST cooling (Figures 6k–6m). For a 180° turning angle, the maximum cooling is located 25 km to the left of the TC track (Figure 6n).

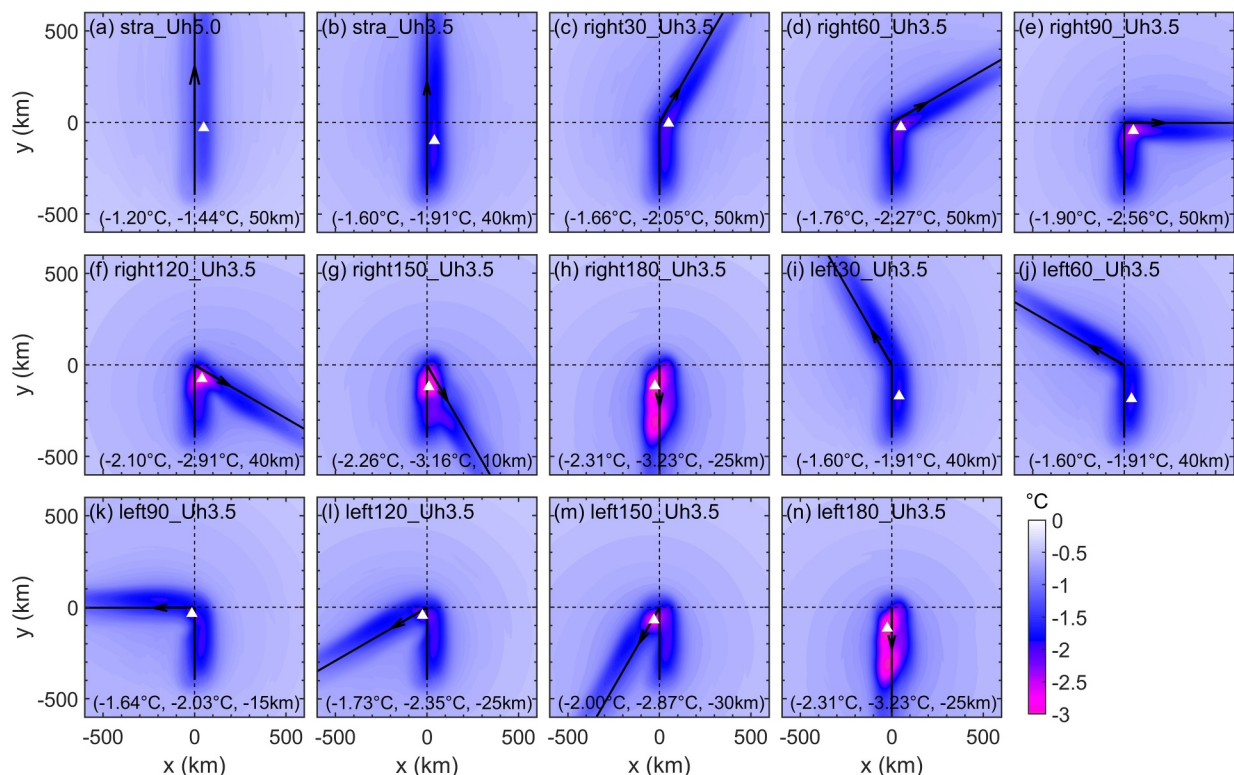


Figure 6. Spatial pattern of simulated TC-induced SSTA. (a) and (b) SSTA induced by the TC that follows a straight path at a constant translation speed of panels (a) 5.0 m s^{-1} and (b) 3.5 m s^{-1} (c)–(h) SSTA induced by the TC that undergoes right turning at a constant translation speed of 3.5 m s^{-1} with the turning angle of 30°–180° in increments of 30°. (i)–(n) Same as panels (c)–(h) but for left turning. The solid black line indicates the track of the TC. The white triangle indicates the minimum SSTA position. The values in parentheses at the bottom indicate the average SSTA within 100 km from the minimum SSTA position (°C), the minimum SSTA (°C), and the x-axis location of the minimum SSTA (km).

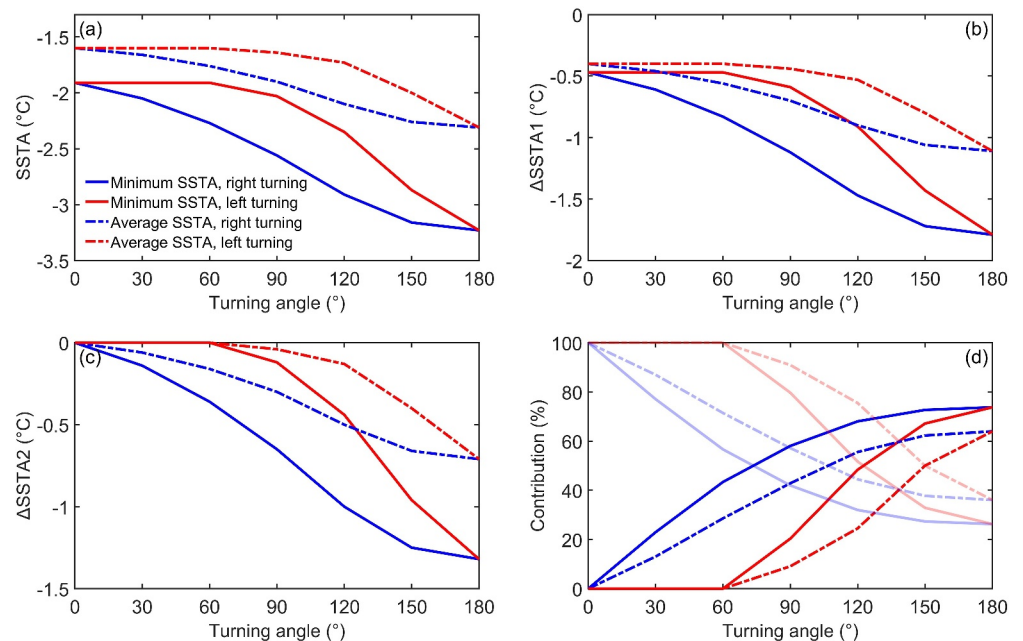


Figure 7. (a) The minimum SSTA (solid lines) and average SSTA (dash-dotted lines) within 100 km from the minimum SSTA position induced by right-turning (blue lines) and left-turning TCs (red lines), respectively. (b) and (c) SSTA difference with the SSTA induced by the straight-moving TC at a constant U_h of (b) 5 m s⁻¹ and (c) 3.5 m s⁻¹. (d) The contribution of track turning (low-transparency lines) and slow translation speed (high-transparency lines) to cooling enhancement. The contribution of track turning is calculated by $\Delta SSTA2/\Delta SSTA1 \times 100\%$. For detailed computations, please refer to Table S1 in Supporting Information S1.

For straight-moving TCs with U_h of 5.0 and 3.5 m s⁻¹, the magnitudes of maximum SST cooling are 1.44°C and 1.91°C, respectively (Figures 6a and 6b), suggesting that slow U_h enhances cooling by 0.47°C. For right-turning TCs, the maximum cooling magnitude increases monotonically with turning angle, ranging from 2.05°C at 30° turning angle to 3.16°C at 150° turning angle (Figures 6c–6h and 7a). For left-turning TCs, the maximum cooling magnitude increases from 1.90°C at 30° turning angle to 2.87°C at 150° turning angle (Figures 6i–6n and 7a). Compared to the straight-moving TC with slow U_h , right-turning TCs with turning angle of 30°–150° enhance the maximum cooling by 0.14–1.25°C, accounting for 23%–72% of the total cooling enhancement due to slow U_h and track turning (Figure 7; Table S1 in Supporting Information S1). Left turning seemingly does not contribute to cooling enhancement for 30°–60° turning angle, but it enhances cooling by 0.12–0.96°C for 90°–150° turning angle, accounting for 20%–67% of the total cooling enhancement. For a turning angle of 180°, the cooling magnitude is increased by 1.32°C due to track turning, accounting for 74% of the total cooling enhancement due to slow U_h and track turning. Overall, cooling enhancement is predominantly attributed to slow U_h at small turning angles. However, when the turning angle exceeds 90° for right-turning TCs, the contribution of track turning (>58%) surpasses that of slow U_h (<42%). Similarly, at a turning angle of 120° for left-turning TCs, the contributions of track turning and slow U_h are comparable (48% vs. 52%).

We also calculate the average SSTA within 100 km from the maximum cooling position to assess the effect of track turning (Figures 6 and 7; Table S1 in Supporting Information S1). The straight-moving TC with slow U_h induces stronger cooling than that with fast U_h (magnitude: 1.60 vs. 1.20°C). With the same slow U_h , right-turning TCs with turning angle of 30°–150° induce strong cooling with magnitude of 1.66–2.26°C, representing an increase of 0.06–0.71°C compared to straight-moving TCs. Right turning contributes 13%–62% of the total cooling enhancement due to slow U_h and track turning, with the contribution of 120° right turning exceeding that of slow U_h (56% vs. 44%). For left-turning TCs, the cooling magnitude remains at 1.60°C for turning angles of 30°–60°, indicating no contribution of left turning to cooling enhancement. For turning angles of 90°–150°, the cooling magnitude increases to 1.64–2.00°C, which represents an increase of 0.04–0.40°C compared to straight-moving TCs, indicating 9%–50% contribution to the total cooling enhancement.

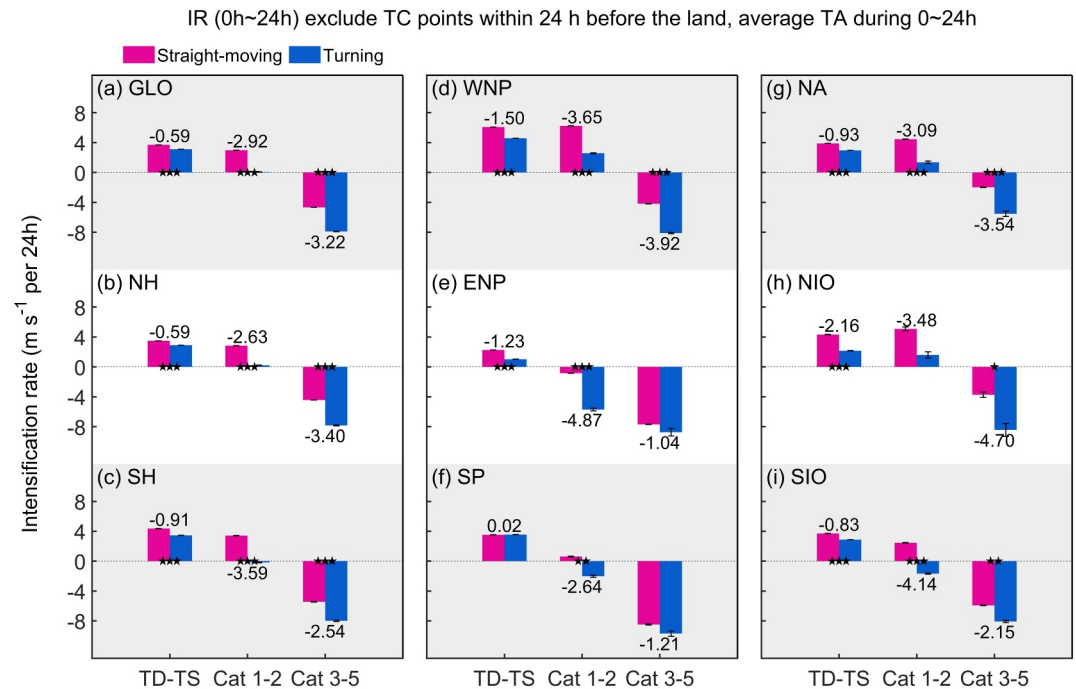


Figure 8. Same as Figure 4, but for TC intensification rate (IR). The IR differences between turning and straight-moving TCs are shown above or behind bars. Since the IR is defined as the maximum wind speed's change in the subsequent 24 hr after passing the current position, the turning angle here used to classify straight-moving and turning TCs is the mean turning angle at successive four track points from the current position.

These results suggest that right turning demonstrates a more pronounced enhancing effect on cooling compared to left turning, which aligns with observations in the NH (Figures 3a–3c). Wind forcing on the right side of TC track is more efficient at producing cooling due to its resonance with near-inertial currents as indicated by rightward-biased cooling in the NH (Price et al., 1994). Furthermore, the cumulative duration of wind forcing by right-turning (left-turning) TCs is longer on the right (left) side of TC track. Therefore, the enhancing effect of right turning is more pronounced than that of left turning. In conclusion, the enhanced SST cooling during slow-moving track-turning stages of TCs is attributed to a combined effect of track turning and slow U_h . The contribution of slow U_h is predominant at small turning angles. However, the contribution of track turning is comparable to or exceeds that of slow U_h when turning angles exceed 90° (120°) for right (left) turning.

3.2. TC Intensification During Track-Turning Stages

3.2.1. TC Intensification Rate

Theoretically, TC-induced SST cooling can reduce air-sea enthalpy flux from the ocean to TCs, thereby suppressing TC intensification (Cione & Uhlhorn, 2003; D'Asaro et al., 2014; Emanuel, 1999; Lin et al., 2013, 2021). To examine the effect of enhanced SST cooling on TC intensification during slow-moving track-turning stages, we compare the IR of turning and straight-moving TCs (Figure 8). Globally, the IR of turning TCs is significantly lower than that of straight-moving TCs for each TC intensity group significantly above the 99% confidence level (Figure 8a). For instance, for categories 1–2 TCs, straight-moving TCs tend to intensify at an average rate of 2.98 m s^{-1} per 24 hr, whereas the intensification of turning TCs is minimal (IR: 0.06 m s^{-1} per 24 hr). Consistent with the global average, turning TCs in each TC-active basin also show lower IR than straight-moving TCs (Figures 8d–8i). Notably, the largest IR difference occurs for categories 1–2 TCs in the ENP (4.87 m s^{-1} per 24 hr) followed by categories 3–5 TCs in the NIO (4.70 m s^{-1} per 24 hr). In both the WNP and NA, IR differences for categories 1–2 and 3–5 TCs exceed global averages of 2.92 and 3.22 m s^{-1} per 24 hr. These results indicate that TC track turning and slow U_h together modulate TC intensification through the negative feedback from SST cooling, that is, an oceanic pathway. However, TC intensification is influenced by multiple factors, and thus its dependence on SST cooling varies across basins. For example, for categories 3–5, TCs in the ENP show the

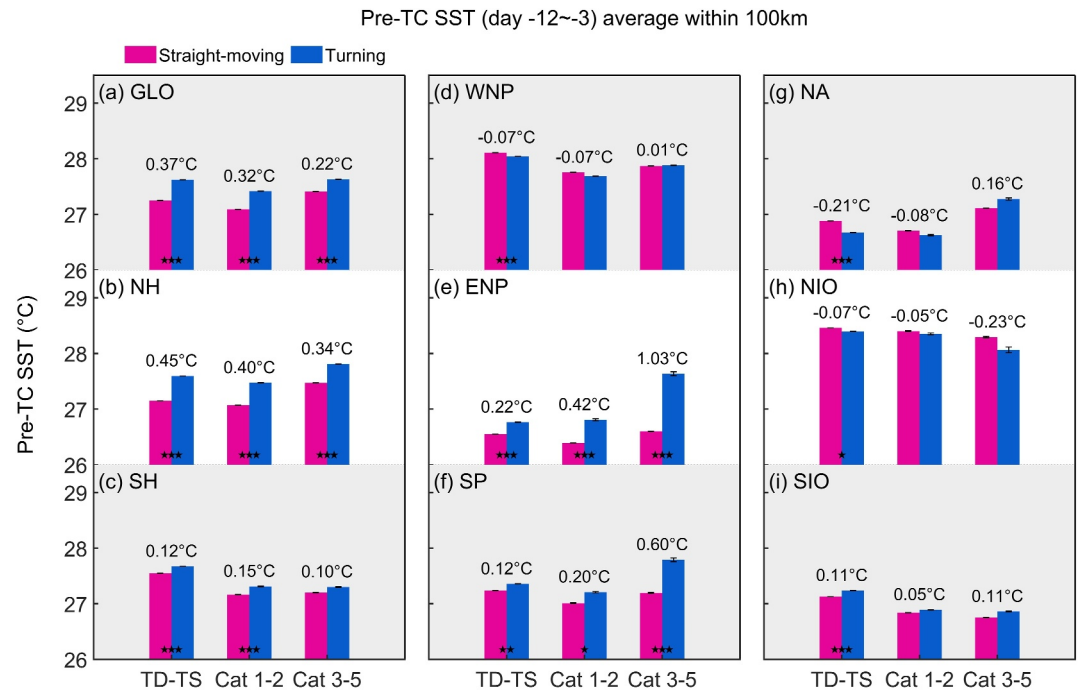


Figure 9. Same as Figure 4, but for pre-TC SST.

largest SSTA difference (Figure 4) but the smallest IR difference (Figure 8) between turning and straight-moving TCs among six TC-active basins. The reduced IR of categories 1–2 TCs during track-turning stages is slightly less pronounced in the NH compared to the SH (2.63 vs. 3.59 m s^{-1} per 24 hr; Figures 8b and 8c) despite stronger cooling enhancement in the NH (Figures 4b and 4c).

In addition to the ocean cooling effect, TC intensification is also influenced by other environmental factors such as pre-TC SST and VWS (Emanuel et al., 2004; C. Gao et al., 2022; Sun et al., 2019), which are also composited here and presented in Figures 9 and 10. Both global and hemispheric averages indicate that the pre-TC SST

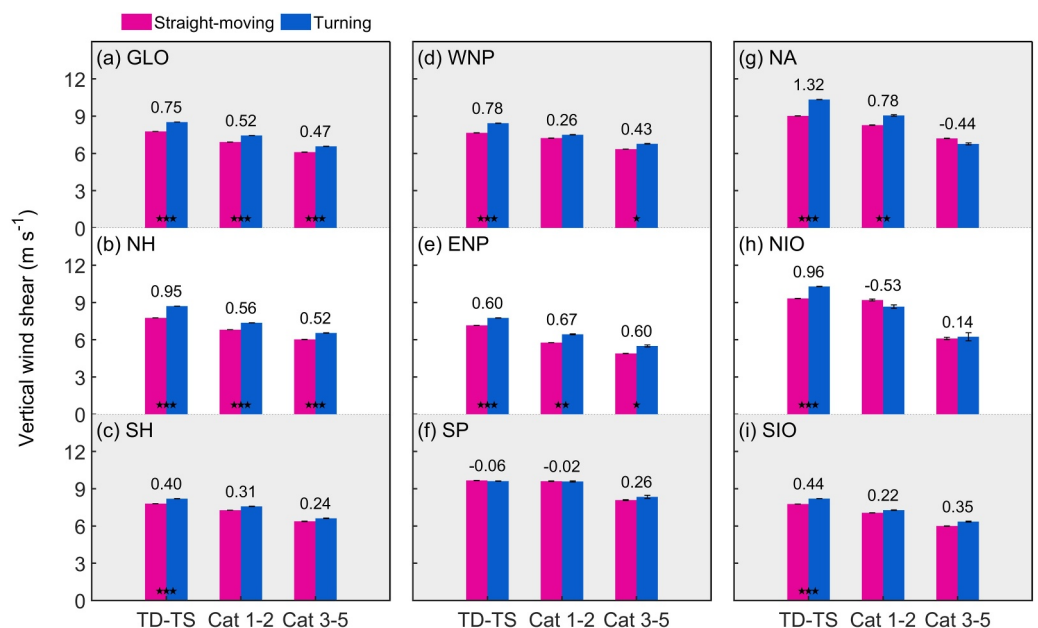


Figure 10. Same as Figure 4, but for vertical wind shear.

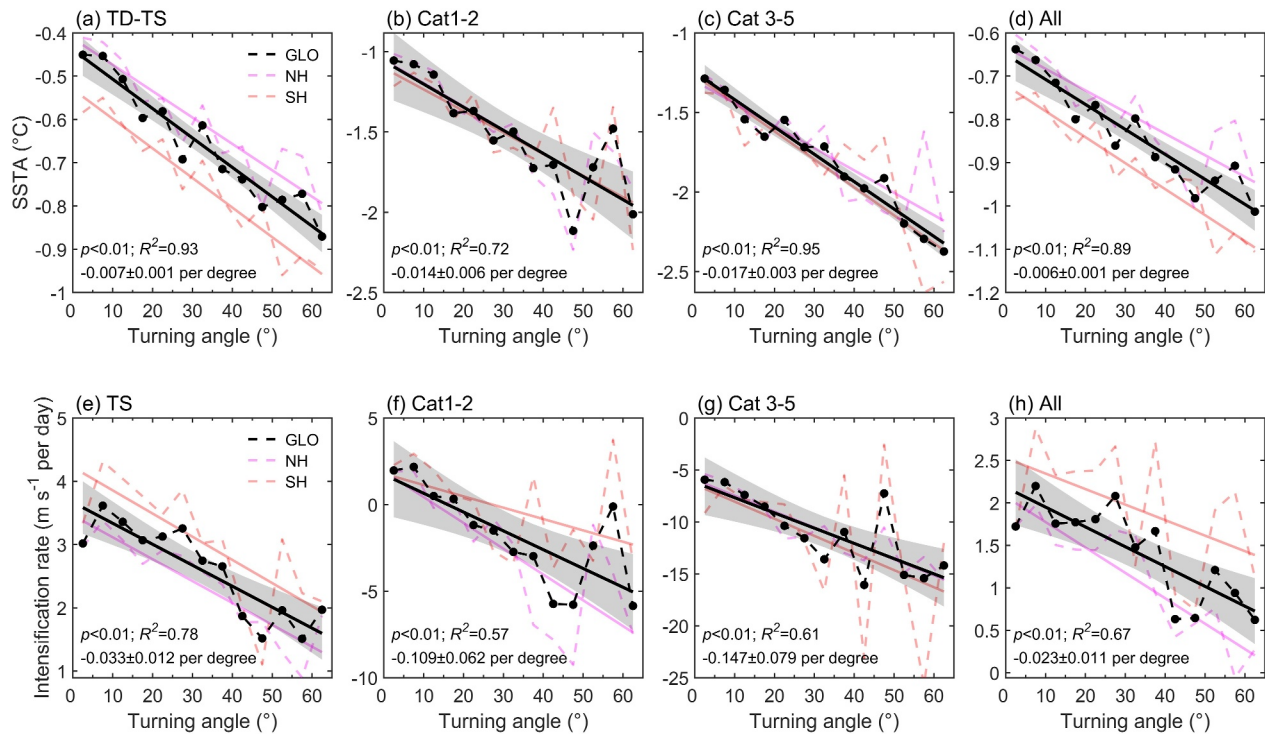


Figure 11. Dependence of TC-induced SSTA and TC intensification rate on turning angle on global and hemispheric averages. (a–d) SSTA as a function of turning angle for TD–TS, categories 1–2, categories 3–5, and all TCs, respectively. Dashed lines denote the composited values. Solid lines and gray shading denote the linear regression trend and the 95% confidence interval. The slope of the linear regression trend, confidence level, and correlation coefficient on global average are shown in the bottom-left corner. (e–h) Same as panels (a–d) but for TC intensification rate.

associated with turning TCs is generally higher than that associated with straight-moving TCs (Figure 9). Higher pre-TC SST during track-turning stages potentially supplies more enthalpy flux to TCs and favors TC intensification (Schade, 2000). In the ENP and SP, turning TCs also exhibit substantially higher pre-TC SST than straight-moving TCs (Figures 7e and 7f). Particularly, for categories 3–5 TCs in the ENP, the pre-TC SST of turning TCs is 1.03°C higher than that of straight-moving TCs. This may explain the smallest IR difference despite the largest SSTA difference in the ENP as noted earlier. In other basins, pre-TC SST differences between turning and straight-moving TCs are mostly small and insignificant. Categories 1–2 TCs in the NH exhibit larger pre-TC SST differences between turning and straight-moving TCs compared to the SH (Figures 9b and 9c). This disparity may offset the suppressing effect of SST cooling to some extent, accounting for the less IR suppression despite stronger SSTA enhancement in the NH. Overall, the higher pre-TC SST associated with turning TCs is favorable for TC intensification and definitely does not explain the lower IR of turning TCs compared to straight-moving TCs.

Vertical wind shear (VWS), an atmospheric dynamical factor, has an inhibiting effect on TC intensification (Frank & Ritchie, 2001). The global average VWS for turning TCs is slightly higher than that for straight-moving TCs (Figure 10). However, the VWS differences between turning and straight-moving TCs are mostly insignificant in TC-active basins such as the NA, SP, and SIO. Therefore, the marginally higher VWS for turning TCs may partially contribute to their suppressed TC intensification, but the extent of its contribution requires future investigation.

A larger TC turning angle combined with slower U_h can lead to a longer residence time or even revisiting of TC wind forcing over local oceans, thereby enhancing SST cooling and negative feedback. Therefore, we further examine the dependence of TC-induced SSTA and TC IR on turning angle (Figure 11). On a global average, both SSTA and IR exhibit a robust decreasing trend as the turning angle increases significantly above the 99% confidence level. For example, with a 10-degree increment of turning angle for categories 1–2 TCs, the SSTA decreases by 0.14°C (R^2 : 0.72) and IR decreases by 1.09 m s⁻¹ per 24 hr (R^2 : 0.57). Consistent with the global

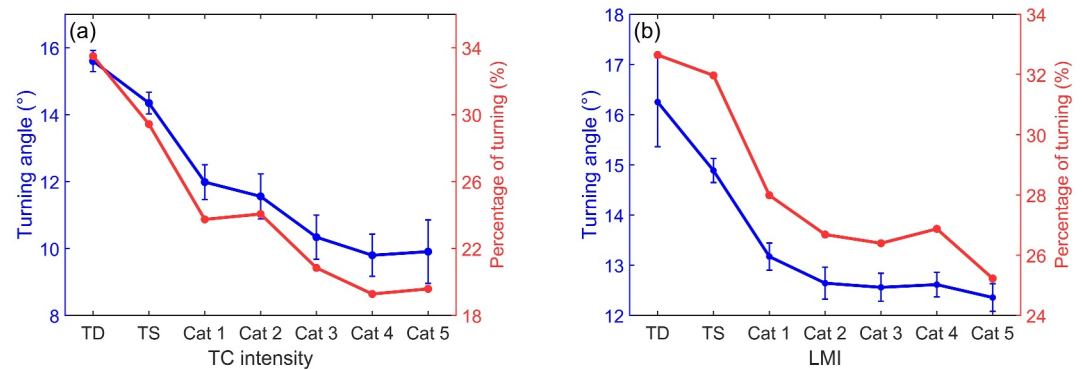


Figure 12. Relationship between track turning and TC intensity on global average. Average turning angle and percentage of track turning as a function of panels (a) TC intensity and (b) TC lifetime-maximum intensity. Error bars indicate the 95% confidence interval.

average, SSTA and IR in both the NH and SH also show a significant decreasing trend with increasing turning angle above the 90% confidence level.

Since a larger turning angle leads to an enhanced cooling effect and weaker TC intensification, TC intensity is expected to be related to the turning angle. Results show that both turning angle and percentage of track turning are generally inversely proportional to TC intensity (Figure 12a). From TD to category 5, the turning angle decreases from 15.6° to 9.9°, and the percentage of track turning decreases from 33.5% to 19.6%. Similarly, both turning angle and percentage of track turning decrease with increasing lifetime-maximum intensity of TCs (Figure 12b). From TD to category 5, the turning angle decreases from 16.3° to 12.4°, and the percentage of track turning decreases from 32.6% to 25.2%. These results suggest that TCs with smaller turning angles or those undergoing less frequent track turning are more likely to develop into intense TCs. For instance, the “Category-6” super typhoon Haiyan (2013) achieved an unprecedented extraordinary intensity of 170 kts, which is partly attributed to its straight tracks throughout its lifespan (Lin et al., 2014).

3.2.2. Rapid Intensification

Rapid intensification (RI), representing extreme intensification of TCs with IR greater than 30 kts ($\sim 15.4 \text{ m s}^{-1}$) per 24 hr, has the potential to substantially increase the destructiveness of TCs (Kaplan & DeMaria, 2003). However, operational forecasts of RI remain challenging to date due to a limited understanding of the factors and mechanisms controlling RI (DeMaria et al., 2021; Kaplan et al., 2010). Considering that TC IR is significantly reduced due to enhanced SST cooling during track-turning stages, RI is also expected to be affected. Results show that the probability of RI is 16.5% for straight-moving TCs on a global average, but it drops to 11.0% for turning TCs (Figure 13a). This decrease of 5.5% accounts for approximately one-third of the RI probability for straight-moving TCs. Among global TC-active basins, the probability of RI during track-turning stages experiences the largest declines in the WNP (7.5%) and NIO (7.4%), followed by the NA (6.4%), whereas the smallest decrease occurs in the ENP (4.6%).

Additionally, we estimate and compare the turning angle and percentage of track turning for RI and non-RI TCs (Figures 13b and 13c). Non-RI TCs are defined as those with IR below 30 kts per 24 hr but greater than zero (Xu & Wang, 2015). On a global average, the turning angle is 14.4° for non-RI TCs but decreases to 11.5° for RI TCs with a difference of 2.9° (Figure 13b). This difference rises to 4.7° in the NIO and 4.2° in the WNP, whereas it is merely 1.6° in the ENP. The percentage of track turning on a global average is 31.8% for non-RI TCs but decreases to 22.6% for RI TCs with a difference of 9.2% (Figure 13c). The largest difference occurs in the NIO and WNP (14.0% and 12.2%), and the smallest difference in the ENP (4.2%). The interbasin differences in track-turning percentage align with those in turning angle. The smallest suppression of RI in the ENP is likely attributable to the lowest probability of track turning (Figure S1 in Supporting Information S1). These results underscore that TC track turning combined with slow U_h is unfavorable for RI. TCs with large turning angles or frequent track turning are more difficult to undergo RI probably due to enhanced SST cooling and negative feedback.

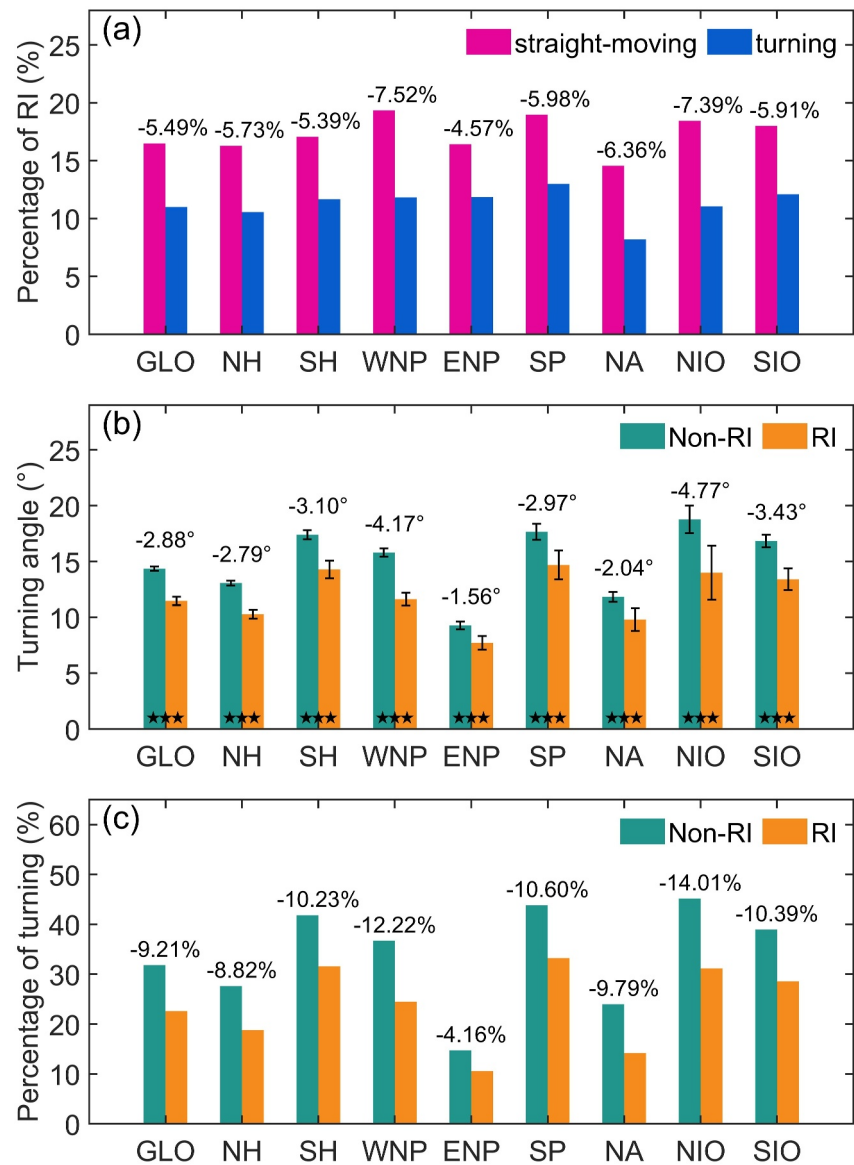


Figure 13. (a) Percentage of RI with respect to intensifying TCs for straight-moving and turning TCs. (b) Average turning angle for RI and non-RI TCs. Error bars indicate the 95% confidence interval. Pentagrams indicate the confidence level of the difference between RI and non-RI TCs: one pentagram suggests the difference is significant above the 90% confidence level, two for 95%, and three for 99% based on the Student's *t* test. (c) Percentage of turning TCs for RI and non-RI TCs. The differences between turning and straight-moving TCs are shown above bars.

4. Discussion

Forecasting of TC track and intensity has always been a key topic in previous studies (e.g., Camargo, 2013; Cangialosi et al., 2020; Cox et al., 2013; DeMaria et al., 2007; Elsberry et al., 2007; K. Gao et al., 2023; Goni et al., 2009; Na et al., 2018; Shi & Xu, 2024). However, the forecasting of TCs with track turning has received limited attention. Previous studies mainly focus on track forecast errors for turning TCs (e.g., Chan et al., 1980). For instance, Chan et al. (1980) reported that forecast errors in turning angle and TC track are larger for turning TCs than for straight-moving TCs based on TCs in the West Indies during 1961–1977. Considering the suppression of TC intensification during track-turning stages via the oceanic pathway, as demonstrated in Section 3.2, it is anticipated that intensity forecast errors will also differ between turning and straight-moving TCs. Nevertheless, the intensity forecasts for turning TCs remain unknown to date.

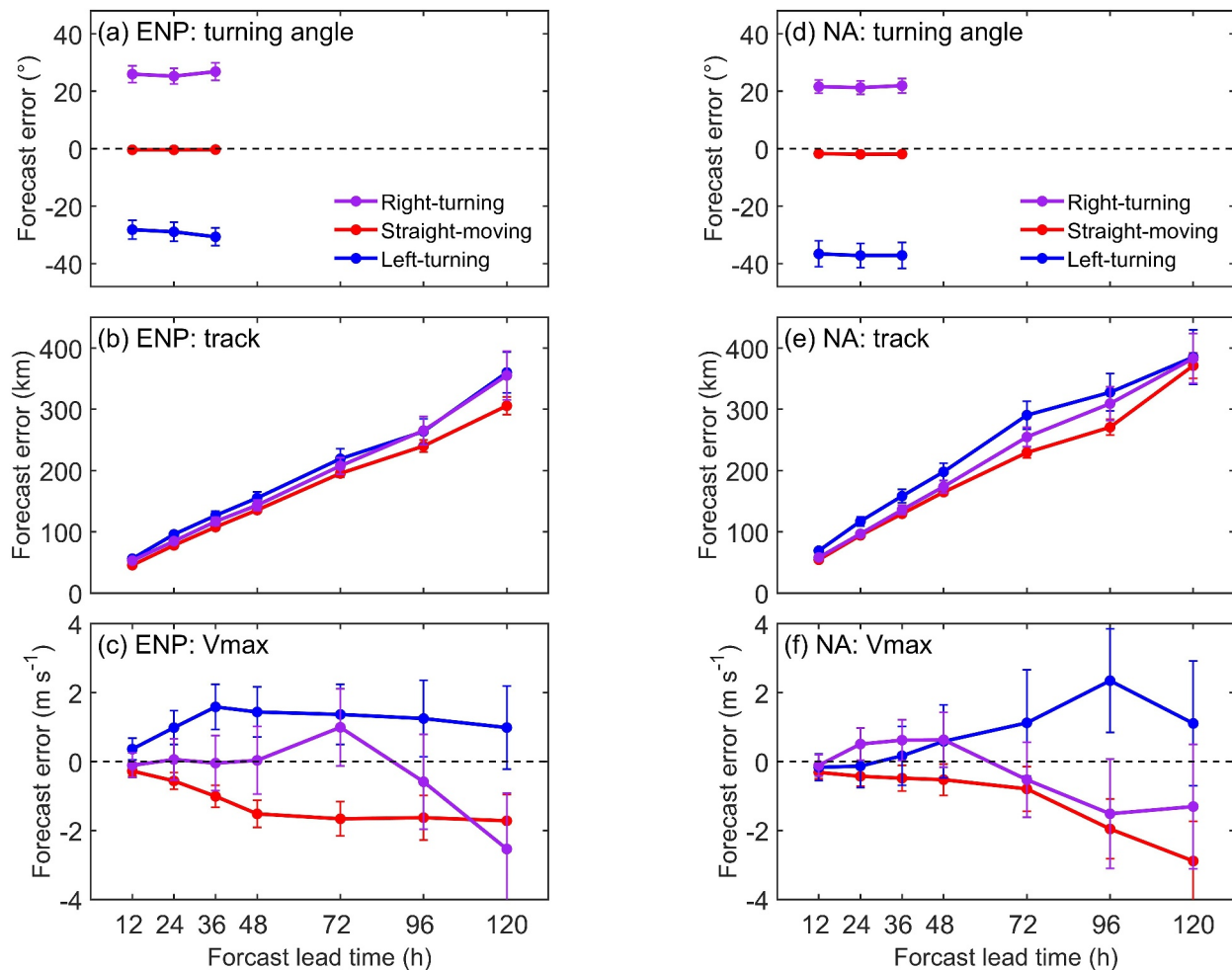


Figure 14. Comparison of forecast errors between turning and straight-moving TCs. Forecast errors in panels (a and d) turning angle, (b and e) track, and (c and f) maximum wind speed as a function of forecast lead time in the panels (a–c) ENP and (d–f) NA. Error bars indicate the 95% confidence level.

The NHC provides operational TC forecast data in the ENP and NA, including forecasts of position and intensity (i.e., V_{\max}). Using these data, we calculate forecast errors in TC turning angle, track, and intensity at forecast lead times of 12, 24, 36, 48, 72, 96, and 120 hr during 1998–2022 (Figure 14). It should be noted that the forecast interval is at least 12 hr. Therefore, we define the turning angle as the difference in direction angle between the current track point and the one 12 hr earlier. Due to the forecast interval increasing to 24 hr after the 48-hr forecast lead time, turning angle forecast errors are not calculated after the 36-hr forecast lead time. A positive (negative) turning angle forecast error indicates that the forecast position is located to the left (right) of the best track position. Results show that turning angle forecast errors are nearly zero for straight-moving TCs, suggesting accurate predictions of TC moving directions (Figures 14a and 14d). However, for left- and right-turning TCs, the respective turning angle forecast errors are approximately -27° and 26° in the ENP and -36° and 21° in the NA, indicating a substantial underestimation of turning angles in TC forecasts. In comparison, turning angle forecast errors during the 1960s–1970s were -50° for left-turning TCs and 38° for right-turning TCs (Chan et al., 1980), demonstrating a notable reduction in turning angle forecast errors in recent years.

Track forecast errors, defined as the distance between the forecast position and the best track position, increase with forecast lead time for both straight-moving and turning TCs (Figures 14b and 14e). Turning TCs exhibit larger track forecast errors than straight-moving TCs, consistent with the findings of Chan et al. (1980). However, the track forecast errors at a forecast lead time of 24 hr (~ 100 km) are considerably smaller than those reported by Chan et al. (1980) (~ 200 km), indicating advancements in TC track forecasts since the mid-1990s (Cangialosi et al., 2020).

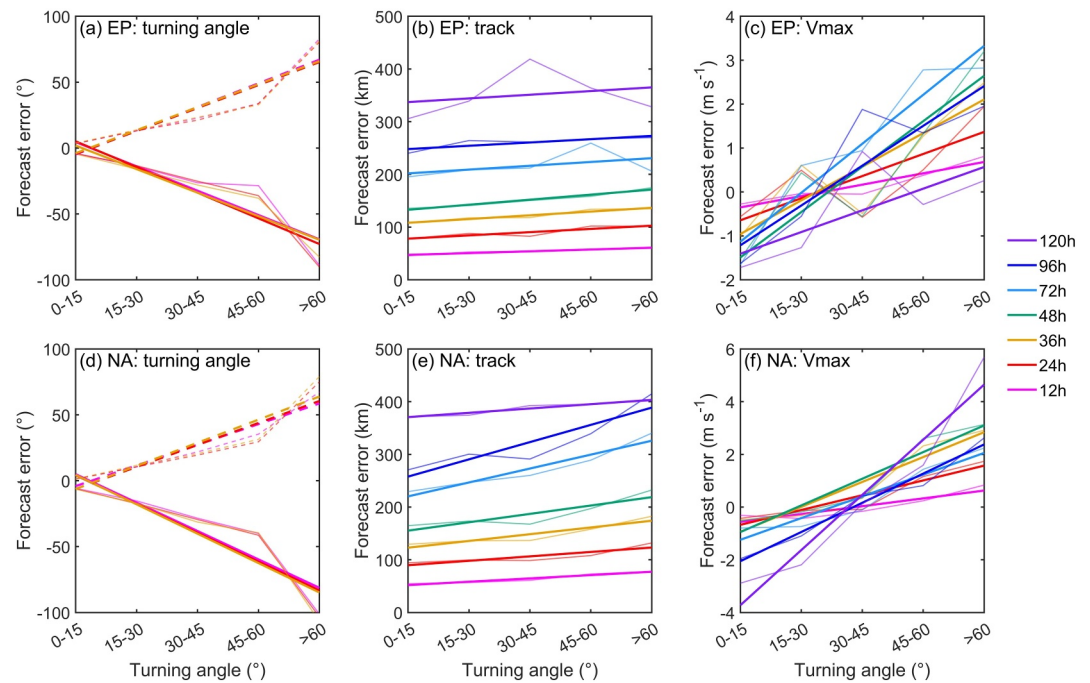


Figure 15. Dependence of forecast errors on turning angle. Forecast errors in panels (a) and (d) turning angle, (b) and (e) track, and (c) and (f) maximum wind speed as a function of turning angle in the panels (a)–(c) ENP and (d)–(f) NA. Solid and dashed lines in panels (a) and (d) indicate left- and right-turning TCs, respectively. Bold straight lines indicate the linear regression trend.

To date, state-of-the-art TC forecast models tend to systematically underforecast TC intensity (e.g., Elsberry et al., 2007; Na et al., 2018; Shi & Xu, 2024). Our results reveal that TC intensity forecast errors from 12 to 120 hr are consistently negative for straight-moving TCs (Figures 14c and 14f), indicating that the forecast intensity is weaker than the best track intensity, confirming the underforecast of intensity. However, for turning TCs, intensity forecast errors are mostly around zero or positive, suggesting that the forecast intensity is close to or stronger than the best track intensity. Notably, in the ENP, the average 36-hr intensity forecast error reaches 1.58 m s^{-1} for left-turning TCs. In the NA, the average 96-hr intensity forecast error reaches 2.35 m s^{-1} for left-turning TCs. The discrepancy in intensity forecast errors between turning and straight-moving TCs is probably because TC track turning is severely underestimated in forecast models, which leads to the omission of suppressed TC intensification during track-turning stages via the oceanic pathway. Interestingly, forecasts for left-turning TCs appear less accurate than those for right-turning TCs, as evidenced by larger forecast errors in turning angle, track, and intensity for left-turning TCs. The reasons behind this intriguing phenomenon warrant future exploration.

Considering that TC IR decreases with increasing turning angle (Section 3.2), intensity forecast errors may also vary with turning angle. Therefore, we further examine the dependence of TC forecast errors on turning angle (Figure 15). Generally, forecast errors of turning angle, track, and intensity all manifest a robust increasing trend as the turning angle increases mostly above the 90% confidence level (Table 2). For instance, for 12-hr forecasts in the ENP (NA), with a 15-degree increment in turning angle, turning angle forecast errors increase by 18.5° (21.6°) for left-turning TCs and 16.0° (15.7°) for right-turning TCs. For 48-hr forecasts in the ENP (NA), intensity forecast errors increase by 1.03 (1.01) m s^{-1} with a 15-degree increment in turning angle. Notably, when turning angles are smaller than 30° , the intensity forecast errors are negative, indicating that forecast models underforecast TC intensity. For turning angles larger than 30° , the intensity forecast errors are generally positive, indicating that forecast models overforecast TC intensity. These results suggest that TC track turning tends to be underestimated to a greater extent at larger turning angles, resulting in larger track and intensity forecast errors. In recent years, TC track forecasting has been gradually improved, whereas intensity forecasting remains challenging (Cangialosi et al., 2020; DeMaria et al., 2007). Our results emphasize that improving forecasts of track

Table 2
Trends of Forecast Errors With TC Turning Angle in the ENP (NA)

TC attributes	Forecast lead time	Slope (per 15°)	p-value	R ²
Turning angle forecast errors (left turning; °)	12 hr	−18.47 (−21.56)	0.049 (0.034)	0.77 (0.82)
	24 hr	−19.49 (−21.84)	0.031 (0.033)	0.83 (0.83)
	36 hr	−17.88 (−22.31)	0.018 (0.039)	0.88 (0.81)
Turning angle forecast errors (right turning; °)	12 hr	17.98 (15.68)	0.029 (0.009)	0.84 (0.93)
	24 hr	17.43 (16.68)	0.028 (0.029)	0.84 (0.84)
	36 hr	17.47 (17.54)	0.030 (0.028)	0.83 (0.84)
Track forecast errors (km)	12 hr	3.40 (6.32)	0.006 (0.006)	0.94 (0.94)
	24 hr	6.14 (8.40)	0.047 (0.050)	0.78 (0.77)
	36 hr	7.10 (12.79)	0.010 (0.023)	0.92 (0.86)
	48 hr	9.59 (15.88)	0.003 (0.045)	0.96 (0.79)
	72 hr	7.22 (26.41)	0.437 (0.009)	0.21 (0.92)
	96 hr	6.26 (32.72)	0.080 (0.033)	0.69 (0.83)
	120 hr	6.97 (8.18)	0.679 (0.009)	0.07 (0.92)
V _{max} forecast errors (m s ^{−1})	12 hr	0.26 (0.30)	0.014 (0.031)	0.90 (0.83)
	24 hr	0.50 (0.56)	0.129 (0.017)	0.59 (0.89)
	36 hr	0.77 (0.94)	0.057 (0.012)	0.75 (0.91)
	48 hr	1.03 (1.01)	0.037 (0.012)	0.81 (0.91)
	72 hr	1.11 (0.82)	0.012 (0.011)	0.91 (0.91)
	96 hr	0.91 (1.11)	0.042 (0.002)	0.80 (0.97)
	120 hr	0.49 (2.09)	0.170 (0.008)	0.52 (0.93)

Note. P-values lower than 0.1, indicating trends are significant above the 90% confidence level, are bold.

turning and simulations of ocean negative feedback to TC intensification during track-turning stages is important for enhancing intensity forecast accuracy, warranting more attention in future TC forecasting.

5. Conclusions

Previous studies have demonstrated that TC attributes (intensity, Uh, and size) can modulate TC-induced sea surface cooling and subsequently influence TC intensification via an oceanic pathway (e.g., Lin et al., 2009; Liu et al., 2023; Lloyd & Vecchi, 2011; Mei et al., 2012; Mei & Pasquero, 2013; Pun et al., 2018; Vincent et al., 2012). Steered by complex environmental flows, TCs frequently undergo track turning, the mechanisms behind which have attracted considerable attention in the literature (e.g., Camargo et al., 2007; Chan et al., 1980). However, the influence of TC track turning on TC-induced SST cooling remains little explored despite a few case studies (e.g., D'Asaro et al., 2014; Li et al., 2021; Pun et al., 2018; H. Zhang et al., 2023; Y. Zhang et al., 2023). Additionally, the effects of modulated cooling on TC intensification remain unknown. Therefore, we investigate SST cooling and TC intensification during track-turning stages of TCs in global TC-active basins during 1998–2022, proposing that a combination of track turning and accompanying slow Uh can modulate storm intensification via an oceanic pathway.

In global oceans, about 30% of TCs have a turning angle larger than 15°, which we define as the threshold for distinguishing between turning and straight-moving TCs, following Chan et al. (1980). Turning TCs are widespread across global TC-active basins. The probability of track turning is higher in the SH than in the NH (38% vs. 26%). Among global TC-active basins, the NIO and SP have the highest probability of track turning, whereas the ENP has the lowest, followed by the NA.

Satellite observations show that turning TCs induce stronger SST cooling and larger cooling area compared to straight-moving TCs. Furthermore, in the NH, right-turning TCs induce stronger maximum SST cooling than left-turning TCs (−0.98°C vs. −0.87°C). In contrast, in the SH, left-turning TCs induce stronger cooling than right-turning TCs (−1.06°C vs. −0.99°C). The cooling area for left- and right-turning TCs is expanded to 1.7 and 2.1

times that of straight-moving TCs in the NH, respectively, and to 1.4 and 1.7 times in the SH. The spatial pattern of TC-induced SSTA is also affected. In the NH, the rightward shift of maximum SST cooling is reduced from 50 km for straight-moving TCs to 20 km for left-turning TCs, greatly diminishing the left-right asymmetry of SSTA. In the SH, the leftward shift of maximum SST cooling is reduced from 40 km for straight-moving TCs to 10 km for right-turning TCs, leading to nearly left-right symmetric SST cooling.

We further compare SSTA averaged within 100 km from the TC center and TC IR between turning and straight-moving TCs at the same TC intensity. Turning TCs induce stronger SST cooling than straight-moving TCs (-1.53°C vs. -1.08°C for categories 1–2 on a global average). The enhanced SST cooling effectively suppresses TC intensification. For instance, IR of turning TCs is 2.92 m s^{-1} per 24 hr lower than that of straight-moving TCs for categories 1–2 on a global average (2.98 vs. 0.06 m s^{-1} per 24 hr). Furthermore, both SSTA and IR manifest a robust decreasing trend as turning angle increases. With a 10-degree increment of turning angle for categories 1–2 TCs, SSTA decreases by 0.14°C and IR decreases by 1.09 m s^{-1} per 24 hr. The probability of rapid intensification for turning TCs is approximately one-third lower than that for straight-moving TCs. As a result, TCs with smaller turning angles or less track turning are more likely to intensify into intense TCs. The enhanced cooling and suppressed TC intensification during track-turning stages are also found in different TC-active basins.

We find that turning TCs are usually accompanied by slow U_h , which is approximately 1.5 m s^{-1} lower than that of straight-moving TCs. Both slow U_h and track turning can prolong the local residence time of TC wind forcing, which facilitates mixing and upwelling, resulting in stronger SST cooling and negative feedback (Densmore et al., 2023; Mei et al., 2012; H. Zhang et al., 2023). We conduct a series of numerical experiments to further separate and quantify the relative contribution of track turning and slow U_h . Results show that the enhanced SST cooling during slow-moving track-turning stages of TCs is attributed to a combined effect of slow U_h and track turning. The contribution of slow U_h is predominant at small turning angles but decreases with turning angle. The contribution of track turning, increasing with turning angle, is comparable to or exceeds that of slow U_h when turning angles exceed 90° (120°) for right (left) turning. Right turning demonstrates a greater enhancing effect on cooling than left turning in the NH, which aligns with observations. Additionally, track turning can influence the spatial position of maximum cooling. In the NH, right turning with turning angles smaller and larger than 120° shifts maximum cooling rightward and leftward, respectively. Left turning with turning angles larger than 90° shifts maximum cooling leftward significantly, leading to a leftward-biased SST response.

We also compare forecast errors of turning and straight-moving TCs in the ENP and NA using operational forecast data issued by the NHC. The moving directions of straight-moving TCs are accurately predicted. However, the forecast positions of turning TCs exhibit significant directional deviations from the best track positions with the underestimation of turning angle ranging from 21° to 36° . Consequently, turning TCs have larger track forecast errors compared to straight-moving TCs. The forecast intensity of straight-moving TCs is smaller than the best track intensity, which is one of the major challenges in state-of-the-art TC forecast models. However, the forecast intensity of turning TCs is close to or exceeds the best track intensity. On average, operational forecast models overforecast TC intensity by up to 1.58 and 2.35 m s^{-1} for left-turning TCs in the ENP and NA, respectively. These forecast errors manifest a robust increasing trend as turning angle increases.

In short, our study proposes an oceanic pathway through which the combination of track turning itself and accompanying slow translation speed modulates TC intensification by enhancing TC-self-induced SST cooling. Although TC track forecasts have made significant advancements in recent years, TC intensity forecasts still exhibit large errors typically manifesting as a systematic underestimation of intensity (Cangialosi et al., 2020; Elsberry et al., 2007; Na et al., 2018). Our results demonstrate that operational TC forecast models overforecast the intensity of turning TCs, likely because track turning is underestimated and the suppressed TC intensification via the oceanic pathway is not well simulated. Therefore, TC track turning poses a considerable challenge to improving TC forecast accuracy. Enhancing forecasts of track turning may contribute to improving intensity forecast accuracy, which requires more attention in future TC operational forecasts.

Data Availability Statement

The TC best track data are obtained from the International Best Track Archive for Climate Stewardship (IBTrACS; Knapp et al., 2010) available at <https://www.ncei.noaa.gov/products/international-best-track-archive>. The SST data are downloaded from the Remote Sensing Systems (REMSS, 2024) available at <https://www.remss>.

com/measurements/sea-surface-temperature/. The wind data are obtained from the ERA5 database distributed by the European Centre for Medium-Range Forecasts (Hersbach et al., 2023) available at <https://cds.climate.copernicus.eu/datasets/reanalysis-era5-pressure-levels?tab=download>. The operational TC forecast data are downloaded from the National Hurricane Center (NHC, 2024) available at <https://www.nhc.noaa.gov/archive/>.

Acknowledgments

This study is supported by the National Natural Science Foundation of China (42476029, 42427805), the National Key Research and Development Program of China (2022RDC2013300, 2022YFC3104304), and the Hainan Province Science and Technology Special Fund (ZDYF2023GXJS151, ZDYF2023GXJS149, SOLZSKY2024009, SOLZSKY2024001).

References

- Balaguru, K., Chang, P., Saravanan, R., Leung, L. R., Xu, Z., Li, M., & Hsieh, J. S. (2012). Ocean barrier layers' effect on tropical cyclone intensification. *Proceedings of the National Academy of Sciences*, 109(36), 14343–14347. <https://doi.org/10.1073/pnas.1201364109>
- Balaguru, K., Foltz, G. R., Leung, L. R., D'Asaro, E., Emanuel, K. A., Liu, H., & Zedler, S. E. (2015). Dynamic potential intensity: An improved representation of the ocean's impact on tropical cyclones. *Geophysical Research Letters*, 42(16), 6739–6746. <https://doi.org/10.1002/2015gl064822>
- Bender, M. A., & Ginis, I. (2000). Real-case simulations of hurricane–ocean interaction using a high-resolution coupled model: Effects on hurricane intensity. *Monthly Weather Review*, 128(4), 917–946. [https://doi.org/10.1175/1520-0493\(2000\)128<0917:RCSOHO>2.0.CO;2](https://doi.org/10.1175/1520-0493(2000)128<0917:RCSOHO>2.0.CO;2)
- Bi, X., Chen, G., Shi, D., Wang, K., & Zhou, W. (2020). A statistical analysis of the influences of multi-timescale waves on tropical cyclone sudden track changes over the Western North Pacific. *Frontiers in Earth Science*, 8, 309. <https://doi.org/10.3389/feart.2020.00309>
- Camargo, S. J. (2013). Global and regional aspects of tropical cyclone activity in the CMIP5 models. *Journal of Climate*, 26(24), 9880–9902. <https://doi.org/10.1175/JCLI-D-12-00549.1>
- Camargo, S. J., Robertson, A. W., Gaffney, S. J., Smyth, P., & Ghil, M. (2007). Cluster analysis of typhoon tracks. Part II: Large-scale circulation and ENSO. *Journal of Climate*, 20(14), 3654–3676. <https://doi.org/10.1175/JCLI4203.1>
- Cangialosi, J. P., Blake, E., DeMaria, M., Penny, A., Latta, A., Rappaport, E., & Tallapragada, V. (2020). Recent progress in tropical cyclone intensity forecasting at the National Hurricane Center. *Weather and Forecasting*, 35(5), 1913–1922. <https://doi.org/10.1175/WAF-D-20-0059.1>
- Chan, J. C. (2005). The physics of tropical cyclone motion. *Annual Review of Fluid Mechanics*, 37(1), 99–128. <https://doi.org/10.1146/annurev.fluid.37.061903.175702>
- Chan, J. C., & Gray, W. M. (1982). Tropical cyclone movement and surrounding flow relationships. *Monthly Weather Review*, 110(10), 1354–1374. [https://doi.org/10.1175/1520-0493\(1982\)110<1354:TCMASF>2.0.CO;2](https://doi.org/10.1175/1520-0493(1982)110<1354:TCMASF>2.0.CO;2)
- Chan, J. C., Gray, W. M., & Kidder, S. Q. (1980). Forecasting tropical cyclone turning motion from surrounding wind and temperature fields. *Monthly Weather Review*, 108(6), 778–792. [https://doi.org/10.1175/1520-0493\(1980\)108<0778:FTCTMF>2.0.CO;2](https://doi.org/10.1175/1520-0493(1980)108<0778:FTCTMF>2.0.CO;2)
- Chen, S. S., Knaff, J. A., & Marks, F. D. (2006). Effects of vertical wind shear and storm motion on tropical cyclone rainfall asymmetries deduced from TRMM. *Monthly Weather Review*, 134(11), 3190–3208. <https://doi.org/10.1175/MWR3245.1>
- Chiang, T.-L., Wu, C.-R., & Oey, L.-Y. (2011). Typhoon Kai-Tak: An ocean's perfect storm. *Journal of Physical Oceanography*, 41(1), 221–233. <https://doi.org/10.1175/2010JPO4518.1>
- Cione, J. J., & Uhlhorn, E. W. (2003). Sea surface temperature variability in hurricanes: Implications with respect to intensity change. *Monthly Weather Review*, 131(8), 1783–1796. <https://doi.org/10.1175/2562.1>
- Cox, J., House, D., & Lindell, M. (2013). Visualizing uncertainty in predicted hurricane tracks. *International Journal for Uncertainty Quantification*, 3(2), 143–156. <https://doi.org/10.1615/int.j.uncertaintyquantification.2012003966>
- D'Asaro, E. A., Black, P. G., Centurioni, L. R., Chang, Y. T., Chen, S. S., Foster, R. C., et al. (2014). Impact of typhoons on the ocean in the Pacific. *Bulletin of the American Meteorological Society*, 95(9), 1405–1418. <https://doi.org/10.1175/BAMS-D-12-00104.1>
- DeMaria, M. (1996). The effect of vertical shear on tropical cyclone intensity change. *Journal of the Atmospheric Sciences*, 53(14), 2076–2088. [https://doi.org/10.1175/1520-0469\(1996\)053<2076:TEOVSO>2.0.CO;2](https://doi.org/10.1175/1520-0469(1996)053<2076:TEOVSO>2.0.CO;2)
- DeMaria, M., Franklin, J. L., Onderlinde, M. J., & Kaplan, J. (2021). Operational forecasting of tropical cyclone rapid intensification at the National Hurricane Center. *Atmosphere*, 12(6), 683. <https://doi.org/10.3390/atmos12060683>
- DeMaria, M., Knaff, J. A., & Sampson, C. (2007). Evaluation of long-term trends in tropical cyclone intensity forecasts. *Meteorology and Atmospheric Physics*, 97(1), 19–28. <https://doi.org/10.1007/s00703-006-0241-4>
- Densmore, C. R., Sanabia, E. R., & Jayne, S. R. (2023). Ocean temperature observations in Hurricane Dorian (2019). *Monthly Weather Review*, 151(6), 1509–1520. <https://doi.org/10.1175/MWR-D-22-0271.1>
- Elisberry, R. L., Lambert, T. D. B., & Boothe, M. A. (2007). Accuracy of Atlantic and Eastern North Pacific tropical cyclone intensity forecast guidance. *Weather and Forecasting*, 22(4), 747–762. <https://doi.org/10.1175/WAF1015.1>
- Emanuel, K. A. (1986). An air–sea interaction theory for tropical cyclones. Part I: Steady-state maintenance. *Journal of the Atmospheric Sciences*, 43(6), 585–605. [https://doi.org/10.1175/1520-0469\(1986\)043<0585:AASITF>2.0.CO;2](https://doi.org/10.1175/1520-0469(1986)043<0585:AASITF>2.0.CO;2)
- Emanuel, K. A. (1999). Thermodynamic control of hurricane intensity. *Nature*, 401(6754), 665–669. <https://doi.org/10.1038/44326>
- Emanuel, K. A. (2003). Tropical cyclones. *Annual Review of Earth and Planetary Sciences*, 31(1), 75–104. <https://doi.org/10.1146/annurev.earth.31.100901.141259>
- Emanuel, K. A. (2005). Increasing destructiveness of tropical cyclones over the past 30 years. *Nature*, 436(7051), 686–688. <https://doi.org/10.1038/nature03906>
- Emanuel, K. A., DesAutels, C., Holloway, C., & Korty, R. (2004). Environmental control of tropical cyclone intensity. *Journal of the Atmospheric Sciences*, 61(7), 843–858. [https://doi.org/10.1175/1520-0469\(2004\)061<0843:ECOTCI>2.0.CO;2](https://doi.org/10.1175/1520-0469(2004)061<0843:ECOTCI>2.0.CO;2)
- Frank, W. M., & Ritchie, E. A. (2001). Effects of vertical wind shear on the intensity and structure of numerically simulated hurricanes. *Monthly Weather Review*, 129(9), 2249–2269. [https://doi.org/10.1175/1520-0493\(2001\)129<2249:EOWVSO>2.0.CO;2](https://doi.org/10.1175/1520-0493(2001)129<2249:EOWVSO>2.0.CO;2)
- Gao, C., Zhou, L., Wang, C., Lin, I. L., & Murtugudde, R. (2022). Unexpected limitation of tropical cyclone genesis by subsurface tropical central-north Pacific during El Niño. *Nature Communications*, 13(1), 7746. <https://doi.org/10.1038/s41467-022-35530-9>
- Gao, K., Harris, L., Bender, M., Chen, J. H., Zhou, L., & Knutson, T. (2023). Regulating fine-scale resolved convection in high-resolution models for better hurricane track prediction. *Geophysical Research Letters*, 50(13), e2023GL103329. <https://doi.org/10.1029/2023GL103329>
- George, J. E., & Gray, W. M. (1977). Tropical cyclone recurvature and nonrecurvature as related to surrounding wind–height fields. *Journal of Applied Meteorology*, 1962–1982(1), 34–42. [https://doi.org/10.1175/1520-0450\(1977\)016<0034:tcraa>2.0.CO;2](https://doi.org/10.1175/1520-0450(1977)016<0034:tcraa>2.0.CO;2)
- Goni, G., DeMaria, M., Knaff, J., Sampson, C., Ginis, I., Bringas, F., et al. (2009). Applications of satellite-derived ocean measurements to tropical cyclone intensity forecasting. *Oceanography*, 22(3), 190–197. <https://doi.org/10.5670/oceanog.2009.78>
- Guan, S., Jin, F. F., Tian, J., Lin, I. L., Pun, I. F., Zhao, W., et al. (2024). Ocean internal tides suppress tropical cyclones in the South China Sea. *Nature Communications*, 15(1), 3903. <https://doi.org/10.1038/s41467-024-48003-y>

- Guan, S., Zhao, W., Huthnance, J., Tian, J., & Wang, J. (2014). Observed upper ocean response to typhoon Megi (2010) in the northern South China sea. *Journal of Geophysical Research: Oceans*, 119(5), 3134–3157. <https://doi.org/10.1002/2013JC009661>
- Guan, S., Zhao, W., Sun, L., Zhou, C., Liu, Z., Hong, X., et al. (2021). Tropical cyclone-induced sea surface cooling over the Yellow Sea and Bohai Sea in the 2019 Pacific typhoon season. *Journal of Marine Systems*, 217, 103509. <https://doi.org/10.1016/j.jmarsys.2021.103509>
- Hersbach, H., Bell, B., Berrisford, P., Biavati, G., Horányi, A., Muñoz Sabater, J., et al. (2023). ERA5 hourly data on single levels from 1940 to present [Dataset]. *Copernicus Climate Change Service (C3S) Climate Data Store (CDS)*. <https://doi.org/10.24381/cds.adbb2d47>
- Jacob, S. D., Shay, L. K., Mariano, A. J., & Black, P. G. (2000). The 3D oceanic mixed layer response to Hurricane Gilbert. *Journal of Physical Oceanography*, 30(6), 1407–1429. [https://doi.org/10.1175/1520-0485\(2000\)030<1407:TOMLRT>2.0.CO;2](https://doi.org/10.1175/1520-0485(2000)030<1407:TOMLRT>2.0.CO;2)
- Jaimes, B., & Shay, L. K. (2010). Near-inertial wave wake of Hurricanes Katrina and Rita over mesoscale oceanic eddies. *Journal of Physical Oceanography*, 40(6), 1320–1337. <https://doi.org/10.1175/2010JPO4309.1>
- Jyothi, L., Joseph, S., P. S., Huber, M., & Joseph, L. A. (2022). Distinct oceanic responses at rapidly intensified and weakened regimes of tropical cyclone Ockhi (2017). *Journal of Geophysical Research: Oceans*, 127(6), e2021JC018212. <https://doi.org/10.1029/2021JC018212>
- Kaplan, J., & DeMaria, M. (2003). Large-scale characteristics of rapidly intensifying tropical cyclones in the North Atlantic basin. *Weather and Forecasting*, 18(6), 1093–1108. [https://doi.org/10.1175/1520-0434\(2003\)018<1093:LCORIT>2.0.CO;2](https://doi.org/10.1175/1520-0434(2003)018<1093:LCORIT>2.0.CO;2)
- Kaplan, J., DeMaria, M., & Knaff, J. A. (2010). A revised tropical cyclone rapid intensification index for the Atlantic and eastern North Pacific basins. *Weather and Forecasting*, 25(1), 220–241. <https://doi.org/10.1175/2009WAF2222280.1>
- Knapp, K. R., Kruk, M. C., Levinson, D. H., Diamond, H. J., & Neumann, C. J. (2010). The international best track archive for climate stewardship (IBTrACS): Unifying tropical cyclone data. *Bulletin of the American Meteorological Society*, 91(3), 363–376. <https://doi.org/10.1175/2009BAMS2755.1>
- Li, J., Yang, Y., Wang, G., Cheng, H., & Sun, L. (2021). Enhanced oceanic environmental responses and feedbacks to super typhoon Nida (2009) during the sudden-turning stage. *Remote Sensing*, 13(14), 2648. <https://doi.org/10.3390/rs13142648>
- Lin, I.-I., Black, P., Price, J. F., Yang, C.-Y., Chen, S. S., Lien, C.-C., et al. (2013). An ocean coupling potential intensity index for tropical cyclones. *Monthly Weather Review*, 141(9), 1878–1882. <https://doi.org/10.1002/mwr.10091>
- Lin, I. I., & Chan, J. C. L. (2015). Recent decrease in typhoon destructive potential and global warming implications. *Nature Communications*, 6(1), 7182. <https://doi.org/10.1038/ncomms8182>
- Lin, I. I., Liu, W. T., Wu, C.-C., Wong, G. T. F., Hu, C., Chen, Z., et al. (2003). New evidence for enhanced ocean primary production triggered by tropical cyclone. *Geophysical Research Letters*, 30(13), 1718. <https://doi.org/10.1029/2003gl017141>
- Lin, I. I., Pun, I. F., & Lien, C. C. (2014). “Category-6” super typhoon Haiyan in global warming hiatus: Contribution from subsurface ocean warming. *Geophysical Research Letters*, 41(23), 8547–8553. <https://doi.org/10.1002/2014GL024281>
- Lin, I. I., Pun, I. F., & Wu, C. C. (2009). Upper-ocean thermal structure and the western North Pacific category 5 typhoons. Part II: Dependence on translation speed. *Monthly Weather Review*, 137(11), 3744–3757. <https://doi.org/10.1175/2009MWR2713.1>
- Lin, I. I., Rogers, R. F., Huang, H., Liao, Y., Herndon, D., Yu, J., et al. (2021). A tale of two rapidly intensifying super typhoons: Hagibis (2019) and Haiyan (2013). *Bulletin of the American Meteorological Society*, 102(9), E1645–E1664. <https://doi.org/10.1175/BAMS-D-20-0223.1>
- Liu, Y., Guan, S., Lin, I. I., Mei, W., Jin, F. F., Huang, M., et al. (2023). Effect of storm size on sea surface cooling and tropical cyclone intensification in the western north Pacific. *Journal of Climate*, 36(20), 7277–7296. <https://doi.org/10.1175/JCLI-D-22-0949.1>
- Lloyd, I. D., & Vecchi, G. A. (2011). Observational evidence for oceanic controls on hurricane intensity. *Journal of Climate*, 24(4), 1138–1153. <https://doi.org/10.1175/2010JCLI3763.1>
- Ma, Z., Lin, Y., Fei, J., Zheng, Y., Chu, W., & Ye, H. (2023). Strengthening cold wakes lead to decreasing trend of tropical cyclone rainfall rates relative to background environmental rainfall rates. *npj Climate and Atmospheric Science*, 6(1), 131. <https://doi.org/10.1038/s41612-023-00460-w>
- Mei, W., & Pasquero, C. (2013). Spatial and temporal characterization of sea surface temperature response to tropical cyclones. *Journal of Climate*, 26(11), 3745–3765. <https://doi.org/10.1175/JCLI-D-12-00125.1>
- Mei, W., Pasquero, C., & Primeau, F. (2012). The effect of translation speed upon the intensity of tropical cyclones over the tropical ocean. *Geophysical Research Letters*, 39(7), L07801. <https://doi.org/10.1029/2011GL050765>
- Na, W., McBride, J. L., Zhang, X., & Duan, Y. (2018). Understanding biases in tropical cyclone intensity forecast error. *Weather and Forecasting*, 33(1), 129–138. <https://doi.org/10.1175/WAF-D-17-0106.1>
- NHC. (2024). Tropical cyclone forecast data [Dataset]. NOAA National Hurricane Center. Retrieved from <https://www.nhc.noaa.gov>
- Potter, H., Drennan, W. M., & Graber, H. C. (2017). Upper ocean cooling and air-sea fluxes under typhoons: A case study. *Journal of Geophysical Research: Oceans*, 122(9), 7237–7252. <https://doi.org/10.1002/2017JC012954>
- Price, J. F. (1981). Upper ocean response to a hurricane. *Journal of Physical Oceanography*, 11(2), 153–175. [https://doi.org/10.1175/1520-0485\(1981\)011<0153:UORTAH>2.0.CO;2](https://doi.org/10.1175/1520-0485(1981)011<0153:UORTAH>2.0.CO;2)
- Price, J. F. (1983). Internal wave wake of a moving storm. Part I. Scales, energy budget and observations. *Journal of Physical Oceanography*, 13(6), 949–965. [https://doi.org/10.1175/1520-0485\(1983\)013<0949:IWWOAM>2.0.CO;2](https://doi.org/10.1175/1520-0485(1983)013<0949:IWWOAM>2.0.CO;2)
- Price, J. F., Sanford, T. B., & Forristall, G. Z. (1994). Forced stage response to a moving hurricane. *Journal of Physical Oceanography*, 24(2), 233–260. [https://doi.org/10.1175/1520-0485\(1994\)024<0233:FSRTAM>3E2.0.CO;2](https://doi.org/10.1175/1520-0485(1994)024<0233:FSRTAM>3E2.0.CO;2)
- Pun, I.-F., Lin, I.-I., Lien, C.-C., & Wu, C.-C. (2018). Influence of the size of Super typhoon Megi (2010) on SST cooling. *Monthly Weather Review*, 146(3), 661–677. <https://doi.org/10.1175/mwr-d-17-0044.1>
- REMSS. (2024). MW optimum interpolated SST data set ver. 5.1 [Dataset]. *Remote Sensing Systems*. Retrieved from <https://data.remss.com/SST/daily/mw/v05.1>
- Schade, L. R. (2000). Tropical cyclone intensity and sea surface temperature. *Journal of the Atmospheric Sciences*, 57(18), 3122–3130. [https://doi.org/10.1175/1520-0469\(2000\)057<3122:TCLASS>2.0.CO;2](https://doi.org/10.1175/1520-0469(2000)057<3122:TCLASS>2.0.CO;2)
- Shay, L. K., Goni, G. J., & Black, P. G. (2000). Effects of a warm oceanic feature on Hurricane Opal. *Monthly Weather Review*, 128(5), 1366–1383. [https://doi.org/10.1175/1520-0493\(2000\)128<1366:EOAWOF>2.0.CO;2](https://doi.org/10.1175/1520-0493(2000)128<1366:EOAWOF>2.0.CO;2)
- Shi, R., & Xu, F. (2024). Improvement of global forecast of tropical cyclone intensity by spray heat flux and surface roughness. *Journal of Geophysical Research: Atmospheres*, 129(8), e2023JD039624. <https://doi.org/10.1029/2023JD039624>
- Shi, R., Zhang, Q., Xu, F., Zhang, X., Lin, Y., & Zhang, J. (2023). Decreasing trend of tropical cyclone-induced ocean warming in recent decades. *Environmental Research Letters*, 18(6), 064013. <https://doi.org/10.1088/1748-9326/acd2ed>
- Sun, J., Xu, F., Oey, L. Y., & Lin, Y. (2019). Monthly variability of Luzon Strait tropical cyclone intensification over the Northern South China Sea in recent decades. *Climate Dynamics*, 52(5–6), 3631–3642. <https://doi.org/10.1007/s00382-018-4341-x>
- Vincent, E. M., Lengaigne, M., Madec, G., Vialard, J., Samson, G., Jourdain, N. C., et al. (2012). Processes setting the characteristics of sea surface cooling induced by tropical cyclones. *Journal of Geophysical Research*, 117(C2), C02020. <https://doi.org/10.1029/2011jc007396>

- Walker, N. D., Leben, R. R., Pilley, C. T., Shannon, M., Herndon, D. C., Pun, I.-F., et al. (2014). Slow translation speed causes rapid collapse of northeast Pacific Hurricane Kenneth over cold core eddy. *Geophysical Research Letters*, 41(21), 7595–7601. <https://doi.org/10.1002/2014gl061584>
- Wang, G., Wu, L., Johnson, N., & Ling, Z. (2016). Observed three-dimensional structure of ocean cooling induced by Pacific tropical cyclones. *Geophysical Research Letters*, 43(14), 7632–7638. <https://doi.org/10.1002/2016gl069605>
- Wang, H., Li, J., Song, J., Leng, H., Wang, H., Zhang, Z., et al. (2023). The abnormal track of super typhoon Hinnamnor (2022) and its interaction with the upper ocean. *Deep Sea Research Part I: Oceanographic Research Papers*, 201, 104160. <https://doi.org/10.1016/j.dsr.2023.104160>
- Webster, P. J., Holland, G. J., Curry, J. A., & Chang, H. R. (2005). Changes in tropical cyclone number, duration, and intensity in a warming environment. *Science*, 309(5742), 1844–1846. <https://doi.org/10.1126/science.1116448>
- Wentz, F. J., Gentemann, C., Smith, D., & Chelton, D. (2000). Satellite measurements of sea surface temperature through clouds. *Science*, 288(5467), 847–850. <https://doi.org/10.1126/science.288.5467.847>
- Wu, L., Ni, Z., Duan, J., & Zong, H. (2013). Sudden tropical cyclone track changes over the western North Pacific: A composite study. *Monthly Weather Review*, 141(8), 2597–2610. <https://doi.org/10.1175/MWR-D-12-00224.1>
- Xu, J., & Wang, Y. (2015). A statistical analysis on the dependence of tropical cyclone intensification rate on the storm intensity and size in the North Atlantic. *Weather and Forecasting*, 30(3), 692–701. <https://doi.org/10.1175/WAF-D-14-00141.1>
- Ye, H., Ma, Z., Fei, J., & Duan, Y. (2023). Evaluation of leftward biased cold wakes induced by tropical cyclones in the North Hemisphere. *Journal of Geophysical Research: Oceans*, 128(12), e2023JC020188. <https://doi.org/10.1029/2023JC020188>
- Zhang, H., Liu, Y., Liu, P., Guan, S., Wang, Q., Zhao, W., & Tian, J. (2023a). Enhanced upper ocean response within a warm eddy to Typhoon Nakri (2019) during the sudden-turning stage. *Deep Sea Research Part I: Oceanographic Research Papers*, 199, 104112. <https://doi.org/10.1016/j.dsr.2023.104112>
- Zhang, J., Lin, Y., Chavas, D. R., & Mei, W. (2019). Tropical cyclone cold wake size and its applications to power dissipation and ocean heat uptake estimates. *Geophysical Research Letters*, 46(16), 10177–10185. <https://doi.org/10.1029/2019GL083783>
- Zhang, X., Xu, F., Zhang, J., & Lin, Y. (2022). Decrease of annually accumulated tropical cyclone-induced sea surface cooling and diapycnal mixing in recent decades. *Geophysical Research Letters*, 49(13), e2022GL099290. <https://doi.org/10.1029/2022GL099290>
- Zhang, Y., Liu, Y., Guan, S., Wang, Q., Zhao, W., & Tian, J. (2023b). Sudden track turning of Typhoon Prapiroon (2012) enhanced the upper ocean response. *Remote Sensing*, 15(2), 302. <https://doi.org/10.3390/rs15020302>